

Review

# Recent Advances in the Application of MOFs in Supercapacitors

Christos Argirasis <sup>1,2,\*</sup>, Maria-Eleni Katsanou <sup>2</sup>, Niyaz Alizadeh <sup>3</sup>, Nikolaos Argirasis <sup>3</sup> and Georgia Sourkouni <sup>2</sup> 

<sup>1</sup> Laboratory of Inorganic Materials Technology, School of Chemical Engineering, National Technical University of Athens, 15773 Athens, Greece

<sup>2</sup> Clausthal Centre of Materials Technology (CZM), Clausthal University of Technology, 38678 Clausthal-Zellerfeld, Germany; maria.eleni.katsanou@tu-clausthal.de (M.-E.K.); cogsa@tu-clausthal.de (G.S.)

<sup>3</sup> MAT4NRG—Gesellschaft für Materialien und Energieanwendungen mbH, Burgstätter Str. 42, 38678 Clausthal-Zellerfeld, Germany; nikos.argirasis@mat4nrg.de (N.A.); niyaz.alizadeh@mat4nrg.de (N.A.)

\* Correspondence: amca@chemeng.ntua.gr

**Abstract:** As the need for energy is constantly increasing and in the long term fossil fuels are not an option because of global overheating due to the greenhouse effect, alternative energy production concepts such as photovoltaics, wind energy, IR energy harvesters etc., have been developed. The problem is that renewable energy sources are stochastic, and therefore there is a need for electrical energy storage either in rechargeable batteries or in high-performance supercapacitors. In this respect, novel materials are needed to meet the challenges that are related to these technologies. Metal–organic frameworks (MOFs) represent highly promising materials for energy storage applications in supercapacitors (SCs) and thus in recent years have become essential for clean and efficient energy conversion and storage. Metal–organic frameworks (MOFs) present numerous benefits as electrocatalysts, electrolyte membranes, and fuel storage materials; they exhibit exceptional design versatility, extensive surface-to-volume ratios, and permit functionalization with multivalent ligands and metal centers. Here we present an overview of MOF-based materials for electrical energy storage using high-performance supercapacitors. This review deals with recent advances in MOF-based materials for supercapacitors. Finally, an outlook on the future use and restrictions of MOFs in electrochemical applications, with focus on supercapacitors, is given.



Academic Editors: Ruizhi Li,  
Manickam Minakshi and Hai Wang

Received: 5 March 2025

Revised: 22 April 2025

Accepted: 23 April 2025

Published: 2 May 2025

**Citation:** Argirasis, C.; Katsanou, M.-E.; Alizadeh, N.; Argirasis, N.; Sourkouni, G. Recent Advances in the Application of MOFs in Supercapacitors. *Batteries* **2025**, *11*, 181. <https://doi.org/10.3390/batteries11050181>

**Copyright:** © 2025 by the authors. Licensee MDPI, Basel, Switzerland. This article is an open access article distributed under the terms and conditions of the Creative Commons Attribution (CC BY) license (<https://creativecommons.org/licenses/by/4.0/>).

## 1. Introduction

It is estimated that the world will need up to 500 EJ/year by 2050. The need for clean and renewable sources of energy is and will continue to be the most compelling task of 21st-century science [1]. The worldwide urbanization and increasing population have led to a substantial rise in the production of greenhouse gases, particularly CO<sub>2</sub>. There is agreement about the need to reduce greenhouse gases and to shift energy production to green and renewable, so-called alternative sources, like photovoltaics and wind energy. As these sources are not producing continuous electrical energy, there is a need for storage of the produced and not immediately used excess electrical energy. This can be realized by using advanced batteries and supercapacitors [2].

As civilization increasingly relies on electricity-based technologies, energy demand will inevitably rise. The sustainable utilization of green (renewable) energy sources, like

solar, wind, and tidal energy, are becoming more common. These energy forms are dependent on natural fluctuations and must be converted into electricity and stored. On the other hand, the decrease in fossil fuel sources and increase of carbon footprint of these sources resulted in the requirement of new and renewable energy.

In recent years, supercapacitors (SCs) have attracted significant interest as an innovative energy storage solution [3,4]. One distinguishes two main types of supercapacitors: electric double layer capacitors (EDLCs) and pseudocapacitors [5]. The materials used in electric double layer capacitors (EDLC) exhibit a high specific surface area, and the charge storage mechanism is based on surface phenomena. This leads to a rapid process that enables high power density and cycling stability, albeit at the cost of lower energy density [6].

Among the two principal storage processes for supercapacitors, the electrochemical double-layer capacitor (EDLC) depends on charge adsorption and desorption at the carbon electrode/aqueous electrolyte interface, without demonstrating a Faradaic reaction within its operational potential range. In the mechanism utilizing the pseudocapacitor principle, energy storage transpires via surface redox processes or Faradaic charge transfer reactions involving transition metal oxides or hydroxides and an aqueous electrolyte [7,8]. Pseudo-capacitors (PCs) were developed by integrating electric double layer (EDL) and Faradaic processes within the electrode materials. The electrochemical properties of PCs encompass Faradaic processes and have a capacitive signature; thus, they do not contain exclusively capacitive or Faradaic characteristics. Pseudocapacitance arises from surface-bound redox reactions and enhances total capacitance [9,10]. The pseudocapacitor is a type of capacitor capable of storing larger charges than EDLCs, providing superior energy density due to redox reactions taking place at the material's surface or within its interior [11]. Electric double-layer capacitors (EDLCs) store charge by accumulating ions at the interface of the electrode and electrolyte, resulting in a high-power density. Pseudocapacitors (PCs) predominantly depend on electron transfer at the electrode/electrolyte interface for charge storage, resulting in a higher energy density than electric double-layer capacitors (EDLCs) [12]. In Figure 1, charge storage processes in EDLCs, PCs, and battery resembling electrodes are presented. The quasi-rectangular cyclic voltammetry curve of PCs resembles capacitive electric double layer feedback; nevertheless, it arises from many Faradaic redox processes with a potential distribution. The redox apex must accurately coincide without any peak-to-peak gap. Given that PCs are not physical storage devices yet exhibit linear GCD curves and nearly rectangular CV profiles akin to EDLC, they may be regarded as a complementary variant of EDLC [9,13].

Metal–organic frameworks (MOFs) represent a novel category of materials that have attracted considerable interest over the past 20 years [14,15]. MOFs are open networks composed of metal-centered secondary building units (SBUs) interconnected by organic linkers, resulting in extensive one-dimensional (1-D), two-dimensional (2-D), or three-dimensional (3-D) structures [16,17]. The impact of incorporating ligands on the chemical stability of MOFs can be demonstrated through the application of density functional theory (DFT) [18]. The structures possess a crystalline character, exhibiting long-range organization. Exceptionally uniform pores or channels are inherently present within the framework, typically accommodating guest entities such as solvent molecules (introduced during the synthesis process) or counter ions that neutralize the overall charges on the framework (resulting from the charged metal nodes) [14,15,19]. In contrast to other porous materials like zeolites and carbons, the essential and distinguishing characteristic of MOFs that makes them unique and highly functional is the ability to achieve a “directed” structure by meticulous selection of metals and organic linkers [20–22]. In comparison to traditional supercapacitor materials, the distinctive characteristics of metal–organic frameworks (MOFs), including their extraordinarily high surface area, adjustable porosity, uniformly structured nano and

microscale cavities, potential for in-pore functionality and external surface modification, excellent thermal stability, and the variety of available metal and functional groups, make them highly appealing for electrical energy storage. Furthermore, an endless array of potential combinations of metal ions and organic linkers enables the synthesis of MOFs with diverse characteristics [23].

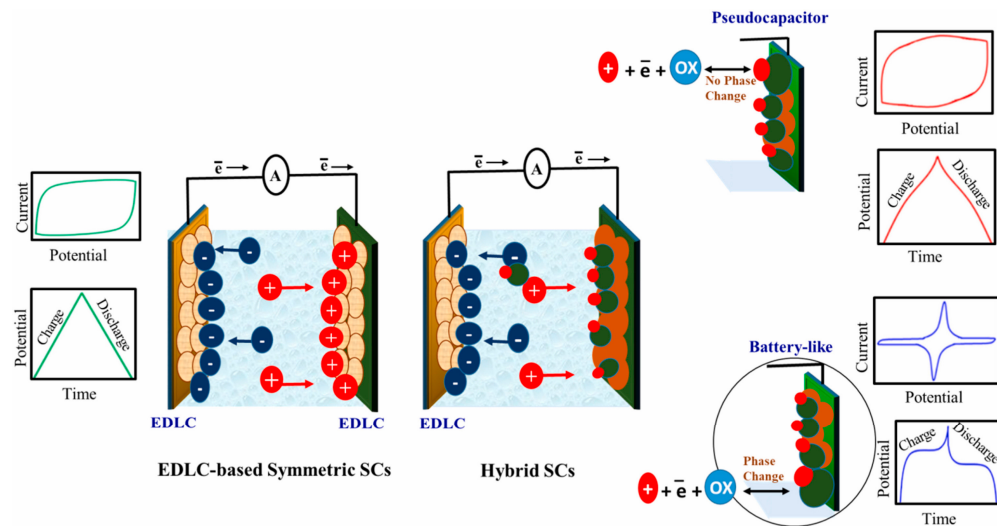


**Figure 1.** Charge storage process in electric double layer capacitors, pseudo capacitors, and battery resembling electrodes. (Reproduced from [9] with permission).

Metal–organic frameworks (MOFs) have the benefit of tunable morphology, enabling the exact synthesis of carbon-based materials with customized structures that exhibit enhanced electrical conductivity, variable porosity, extensive surface area, and robust stability [24]. Consequently, bimetallic MOFs have attracted significant scientific attention due to their remarkable electrical conductivity, strong structural stability, and straightforward production. Liang and coworkers [25] employed a hydrothermal technique to synthesize  $Ni_nCo_m$  MOFs characterized by a layered and channelized structure. The capacitance of  $Ni_1Co_1$  MOF is  $1333 \text{ F g}^{-1}$  at  $2 \text{ A g}^{-1}$ , with  $Ni_1Co_1$  MOF//AC demonstrating a high energy density of  $28 \text{ Wh/kg}$  at  $444 \text{ W kg}^{-1}$ . This value exceeds the capacitance of the individual metal MOFs (Ni-MOF and Co-MOF). The bimetallic oxide  $ZnCo_2O_4$  synthesized from bimetallic cobalt-based metal–organic frameworks (MOFs) offers a 300% higher specific capacity compared to  $Co_3O_4$  generated from MOF along with improved stability [26]. Zhao and coworkers [27] have prepared iron-cobalt oxide nanowires strongly bound on gold-modified porous carbon nanosheets (CPCN) derived from the bimetallic MOFs. A three-electrode design demonstrated exceptional electrochemical performance. The FCO/Au/CPCN@CC electrode exhibits a consistent cyclic voltammetry profile at  $4800 \text{ mV s}^{-1}$ , achieving a peak energy density of  $1090.8 \text{ W h kg}^{-1}$  at  $571.43 \text{ W kg}^{-1}$ , and an energy density of  $344.89 \text{ W h kg}^{-1}$  at the maximum power density of  $4000 \text{ W kg}^{-1}$ . After 10,000 cycles of GCD, the capacitance ratio is 84.27%.

Optimizing the architectures, compositions, and morphologies of MOFs is very important for enhancing the supercapacitor performance. Otun et al. [28] employed a ligand-engineering technique to synthesize ZnCo-bimetallic MOFs with distinct characteristics utilizing three different ligands (2-methylimidazole, terephthalic acid, and 2-amino terephthalic acid) under a uniform synthesis process. The disparity in the electron-donating capacity of the three ligands resulted in alterations to their structural, morphological, and electrochemical characteristics. In comparison to other metal–organic frameworks (MOFs), the imidazole-based ZnCo-MOF (ZnCo-MOF-HMIM), characterized by its dodecahedral

morphology, substantial specific surface area, and mild pore attributes, offers significant electron transport pathways for ion migration at the electrode surface, hence ensuring enhanced charge storage capacity.

Besides the classical solvothermal preparation method [29], several green synthesis methods [30] became in recent years more and more attractive [31]. Methods like electrochemical [32], sonochemical [33,34], microwaves [35], and mechanochemical [36,37] often resulting to different properties and micro-structure of the same MOF [31,38], have been used for the preparation of MOF and descendant products [39].

While the solvothermal method is considered the easiest to use in the lab, as it needs only a furnace, the duration of the solvothermal preparation method is very long (often more than 1 day). Therefore, microwave reactors are often used as they reduce the reaction time from days down to hours. The fastest MOF preparation method is the sonochemical method (Figure 2), as the reaction time is sometimes reduced to less than 1 h [40].

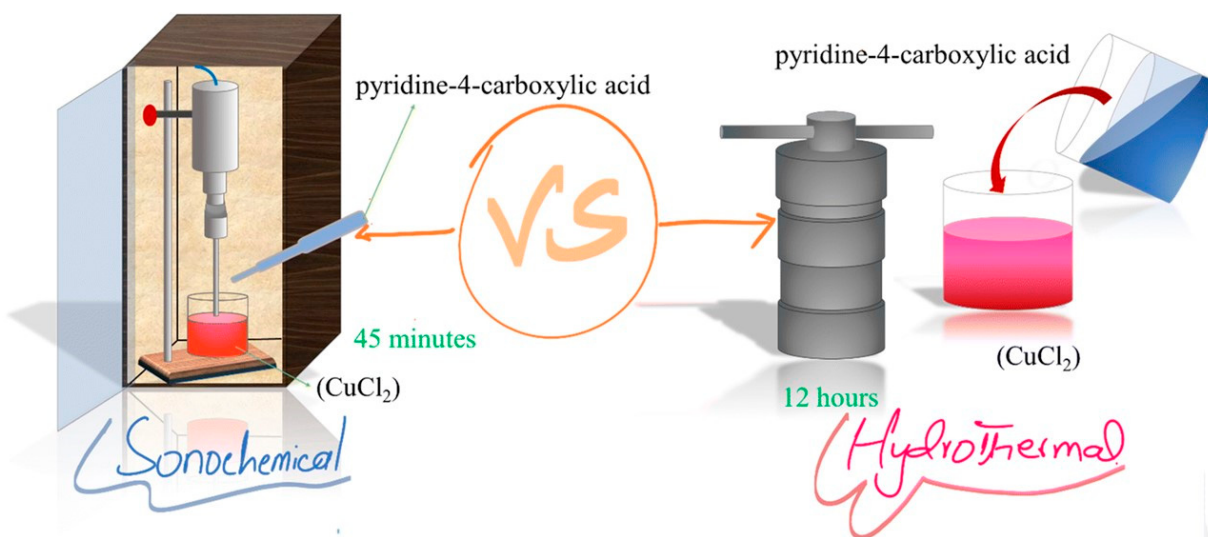


**Figure 2.** Synthesis of Cu-MOF through the hydrothermal and sonochemical approach. (Reproduced from [39] with permission).

The sonochemical method produces differently shaped powders that are mostly finer structured than the ones made using the conventional solvothermal method (Figure 3).

Metal–organic frameworks (MOFs) offer suitable space for electrochemical reactions and ion storage/transfer due to their extensive surface area, making them highly attractive candidates for electrochemical catalysis and energy storage (Figure 4). Compared to other porous materials such as activated carbon and zeolites, MOFs exhibit enhanced architecture and functionalities. Nonetheless, the low conductivity (less than  $10^{-10} \text{ S cm}^{-1}$ ) of most MOFs impedes their practical electrochemical applications, necessitating enhancement. Materials having a high density of charge carriers can function as metallic conductors or semiconductors [41,42]. MOF materials offer significant potential for enhancing electronic and ion conductivity due to their functional pore surface, high surface areas, and extensive structural tunability [43,44]. A review on the development of conductive MOFs can be found in [45]. A review on comprehensive enhancement strategies for electronically and ionically conductive MOFs, as well as recent research progress, is given by Zhang and coworkers [41].

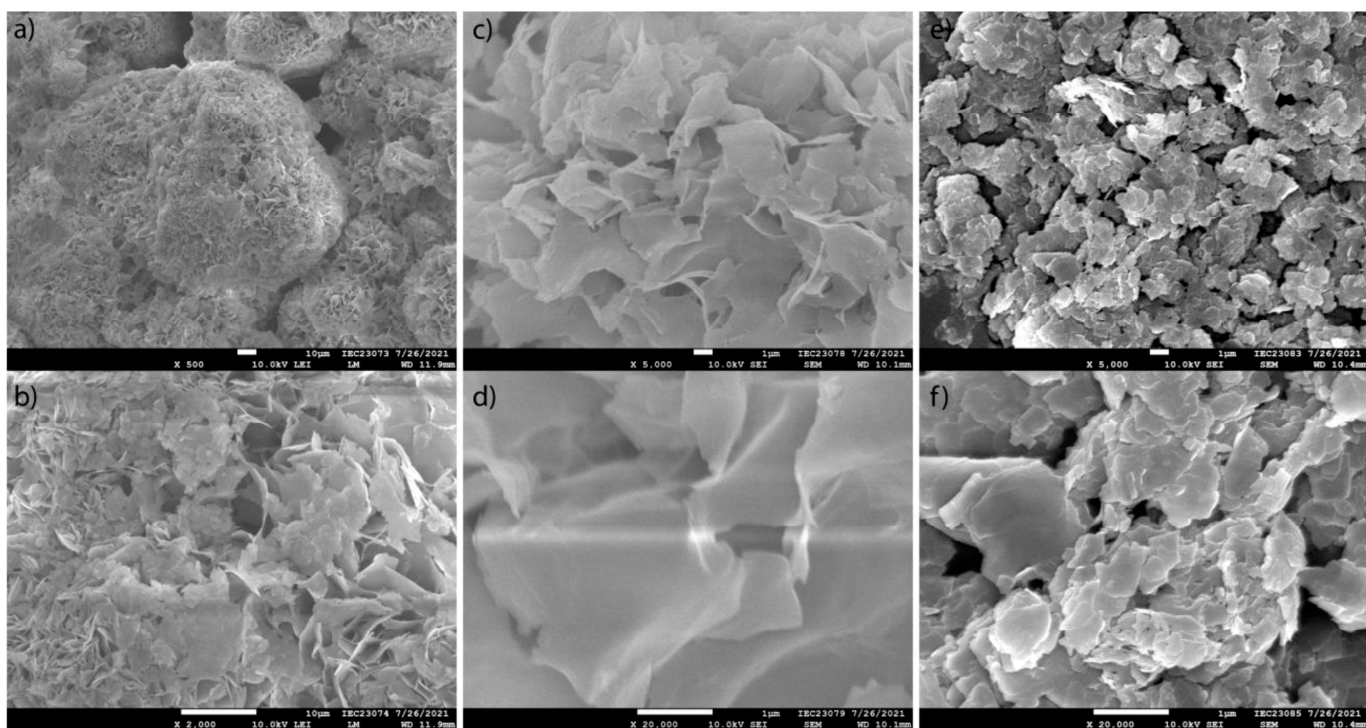


**Figure 3.** SEM images of Zn-adp prepared via (a–d) conventional and (e,f) sonochemical synthesis. (Reproduced from [38] with permission).

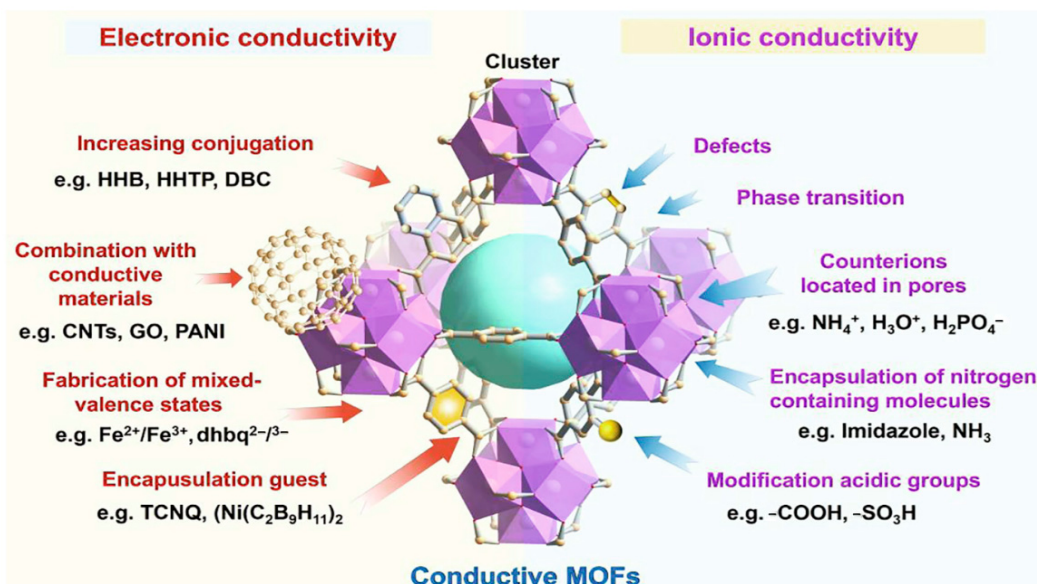


**Figure 4.** Schematic illustrations of the MOF materials as a versatile platform for electronic conduction and ionic conduction. (Reproduced from [41] with permission).

The extensive research on metal–organic frameworks (MOFs) in the last 10 years has resulted in the publication of over 20,000 papers [46]. Theoretical approaches are often employed alongside experimental characterization techniques to investigate newly synthesized materials and elucidate their properties at the microscopic level. Computational methods, alongside various experimental techniques, have been widely employed for the characterization and elucidation of the properties of MOFs. The mathematical simulation of functionalized metal–organic frameworks (MOFs) for energy and catalytic applications encompasses four primary objectives: (i) elucidating the structure and potential post-modification structural alterations of these materials and their correlation to reactivity;

(ii) comprehending the energetics and intricacies of chemical dynamics at catalytic sites, including the modeling of potential energy surfaces for competing mechanisms; (iii) uncovering and elucidating fundamental structure–function relationships that may facilitate further catalyst discovery; and (iv) forecasting novel materials with enhanced catalytic properties [47]. Coudert and Fuchs [48] examine methods for predicting crystal structures, geometrical properties, and conducting large-scale screenings of theoretical MOFs, in addition to their thermal and mechanical properties. A comprehensive analysis of numerous MOFs may yield insights into structure–function relationships. These relationships can be utilized by synthetic chemists for the targeted synthesis of novel materials, or by computational chemists for the optimization of specific properties through extensive computational screening studies, potentially resulting in the discovery of new functional MOFs [49].

The quantum mechanics method (QMM), namely Kohn–Sham (KS) density functional theory (DFT) and different post-Hartree–Fock (Post-HF) approaches, is too expensive for large systems [50]. The computational modeling of MOFs, particularly for large-scale high-throughput screening, is predominantly performed using the molecular mechanics method (MMM), which relies on forcefield parameters. This approach utilizes fitted experimental data or high-level quantum mechanical molecular (QMM) results as the energy expression for the potential energy surface (PES) [51]. This forcefield-based approach eliminates the need for time-intensive self-consistent iterations, resulting in a significant increase in speed. Hai and Wang [52] assert that the theoretical examination of electron motion phenomena must be grounded on Quantum Mechanical Models, such as Density Functional Theory (DFT) or Hartree–Fock (HF).

Despite the increasing computational power, the vast MOF material space necessitates more efficient methodologies for the computational identification of potential MOFs in terms of time and effort. Utilizing data-driven scientific methodologies can provide significant advantages, including expedited design and discovery processes for metal–organic frameworks (MOFs) through the development of machine learning (ML) models and the analysis of intricate structure–performance correlations that surpass expert intuition [53]. ML could also help to identify materials compositions for the improvement of SC electrodes and their combination to more efficient supercapacitors.

The scope of the presented manuscript is to give an overview of recent advances in the use of MOFs in electrochemical devices for electrical energy storage in high-performance supercapacitors. Significant obstacles, limitations for large-scale MOF applications, and prospective developments of MOF-based conductors are also examined.

## 2. MOF-Based Materials for Supercapacitors

Supercapacitors are nowadays accepted as a viable energy storage solution due to their distinctive characteristics, including rapid charge and discharge rates, high power density, and enhanced cycle efficiency in comparison to rechargeable batteries. Furthermore, SCs are environmentally sustainable devices, rendering them suitable for the demands of sustainable energy storage systems. A supercapacitor, akin to other electrochemical systems, comprises two electrodes, an inorganic (aqueous) or organic electrolyte, and a separator. Electrodes are essential for regulating the performance of the supercapacitor and may be uniform in symmetric cells or distinct in asymmetric cells. Furthermore, high conductivity is essential for high-performance supercapacitor electrode materials. Temperature stability, large specific surface area, pore size distribution optimization, manufacturing ease, corrosion resistance, and cost-effectiveness are all factors to be considered. The choice of suitable materials and the refinement of electrode design are essential approaches to enhance the effectiveness of supercapacitors as energy storage devices [54].

Metal–organic frameworks (MOFs), as highly porous and crystalline solids, have demonstrated incredible value as models for synthesizing functional materials suitable for the fabrication of positive electrodes in supercapacitors (SCs) [55,56]. This is primarily attributable to their extensive surface area, adjustable pore size, diverse synthetic methodologies, potential for post-synthetic modification, and the feasibility of scalable production for specific types [57,58]. Nonetheless, their inadequate electrical conductivity and hindrance to ion insertion remain significant obstacles to the direct utilization of MOFs as supercapacitor electrodes [59]. Structural stability is a further challenge, as metal–organic frameworks (MOFs) typically lack stability in conventional electrolyte solutions used in supercapacitors (SCs). Consequently, MOF composites compared to single metal or bimetallic MOFs, typically reduce disparity by providing adjustable electrochemical activity, enhanced charge capacity, and superior electrical conductivity [60]. However, the research on MOF composites incorporating metal oxides or sulfides/phosphides for such purposes remains sparse. Conversely, composites generated from MOFs have gained significantly greater popularity by utilizing their initial captivating morphologies for templated synthesis [61–63].

Li and colleagues [64] offer significant insights into the development and preparation of high-performance HSC-positive electrode materials for practical applications. They have successfully created self-assembled carbon-coated multinuclear Ni<sub>9</sub>S<sub>8</sub>@C-5 composites utilizing spherical Ni-MOF as a structural template through a straightforward high-temperature sulfuration process, demonstrating excellent battery-type energy storage characteristics. (1) The oxidation-rich multinuclear Ni<sub>9</sub>S<sub>8</sub> exhibits significant redox activity, establishing a solid foundation for redox reactions in electrode materials; (2) The development of the spherical outer carbon layer effectively prevents structural collapse and agglomeration of Ni<sub>9</sub>S<sub>8</sub> crystals, thereby improving its structural stability; (3) The Ni-MOF-derived carbon skeleton, characterized by a specific surface area of 132.66 m<sup>2</sup>g<sup>-1</sup> and a mesoporous structure of 3–6 nm, is well-suited for electrochemical reactions and substance transport diffusion. Ni<sub>9</sub>S<sub>8</sub>@C-5 demonstrates impressive specific capacity (278.06 mAh g<sup>-1</sup> at 1 Ag<sup>-1</sup>) and remarkable cycling stability (capacity retention of 88.97% over 5000 cycles). The constructed Ni<sub>9</sub>S<sub>8</sub>@C-5//CTP-AC HSC exhibits an energy density of 69.32 Whkg<sup>-1</sup> at a power density of 800.06 Wkg<sup>-1</sup>, surpassing the values of previously documented MOF-derived nickel sulfide compounds [65–67].

## 2.1. MOFs and Metal Oxides

The synthesis of MO@MOF composites is intricate, necessitating precise conditions to attain uniform metal oxide distribution and robust interfacial contact. Moreover, the addition of metal oxides may diminish the entire porosity of the MOF by obstructing pores, potentially constraining its efficacy in adsorption-based applications. Furthermore, synthesis approaches such as hydrothermal or microwave-assisted procedures might be expensive for energy consumption and equipment, presenting obstacles for large-scale manufacturing. Nonetheless, Metal-oxide@MOF (MO@MOF) composites provide considerable benefits in diverse applications but accompanied by certain obstacles. The use of metal oxides improves the stability of MOFs, rendering the composites appropriate for elevated temperatures and more rigorous environments. This combination enhances catalytic activity by increasing the number of active sites, which is beneficial for pollutant degradation, energy storage, and photocatalysis. Moreover, MOFs provide substantial surface area and porosity, whereas metal oxides impart distinctive capabilities, including electrical, optical, and magnetic properties, hence expanding their applicability in domains such as sensors, batteries, and supercapacitors [68].

The first attempt to create a MOF–oxide composite for supercapacitor applications utilized SnO<sub>2</sub> quantum dots, which were deposited on ZIF-8 by an *in situ* epoxide pre-

cipitation technique [69].  $\text{SnO}_2$  exhibits excellent chemical stability, transparency, and both optical and electrical properties, with prior studies demonstrating that quantum dots demonstrate pronounced oxidation and reduction peaks, signifying that Faradaic processes are involved [70]. The capacitance properties of the composite electrode ( $931 \text{ F g}^{-1}$ ) were better than those of pristine ZIF-8 ( $99 \text{ F g}^{-1}$ ) and  $\text{SnO}_2$  quantum dots ( $241 \text{ F g}^{-1}$ ), achieving about  $500 \text{ F g}^{-1}$  after 500 cycles.

Subsequently, attempts were undertaken utilizing manganese oxide, an interesting metal oxide with a high theoretical specific capacity ( $1370 \text{ F g}^{-1}$ ) and widely recognized in electrochemistry [71], to develop NiO-Ni-r-Graphene Oxide composites [72], as well as Prussian blue (PB) analog composites [56,73].  $\text{MnO}_x$  flower-like structures were synthesized *in situ* on manganese hexacyanoferrate nanocubes through the incorporation of  $\text{NH}_4\text{F}$ , resulting in a fourfold increase in specific capacitance ( $1200 \text{ F g}^{-1}$ ) relative to the pure MOF [74]. The composite had promising outcomes in a flexible supercapacitor, achieving an areal capacitance of  $175 \text{ mF cm}^{-2}$  at  $0.5 \text{ mA cm}^{-2}$ , surpassing the performance of other comparable materials available at that time. In a similar manner, oxide nanolayers were produced on the Prussian Blue microcubes [73] using chemical immersion deposition with  $\text{KMnO}_4$  and PEG (polyethylene glycol) for the reduction reaction. The ASC utilizing a hybrid positive electrode and polyaniline (PANI)/graphene nanoplatelets demonstrated an energy density of  $16.5 \text{ Wh kg}^{-1}$  at  $550 \text{ W kg}^{-1}$  ( $1 \text{ A g}^{-1}$ ). Furthermore, EIS study demonstrated favorable and stable performance for at least 4000 cycles.

Carbon fabric is often used in electrochemical applications, facilitating either the deposition of the catalyst or its *in situ* growth.  $\text{Co}_3\text{O}_4$  was directly synthesized on carbon cloth, which was subsequently immersed in the MOF precursor solution to fabricate core-shell  $\text{Co}_3\text{O}_4/\text{Ni-BDC}$  [75]. The hybrid battery-SC with the layered structure-based positive electrode demonstrated superior specific capacity ( $209 \text{ mAh g}^{-1}$ ) with a retention of 90% over 3000 cycles, in contrast to the sample lacking the oxide ( $154 \text{ mAh g}^{-1}$ ) at  $1 \text{ A g}^{-1}$ . Recently, Zhang et al. [76] altered the cobalt oxide synthesis by calcining ZIF-67, resulting in ribbon-like  $\text{Co}_3\text{O}_4$  nanoarrays (Figure 5).

Binary metal oxides have been intensively investigated for energy storage applications due to their structural stability and commendable reversible capacity [77,78].  $\text{NiCo}_2\text{O}_4$  is environmentally friendly and has proven effective as an electrode option owing to its ability to facilitate battery-type Faradaic redox processes [79], while exhibiting superior electronic conductivity compared to both cobalt and nickel oxide [80]. A straightforward solvothermal method was employed to synthesize core-shell  $\text{NiCo}_2\text{O}_4@\text{Ni-MOF}$  electrodes, utilizing carbon cloth as the substrate for the growth of Ni-BDC nanosheets on  $\text{NiCo}_2\text{O}_4$  nanowires (NWs) [81]. The composite exhibited a substantial areal capacitance of 7.2 and  $5 \text{ F cm}^{-2}$  at current densities of 5 and  $30 \text{ mA cm}^{-2}$ . Additionally, the bimetallic oxide was employed to synthesize  $\text{NiCo}_2\text{O}_4@\text{polypyrrole}$  as the negative electrode for a hybrid supercapacitor, demonstrating encouraging outcomes with approximately 87% retention after 5000 cycles.

Xiong et al. [82] synthesized a nickel-based composite to mitigate disorderly arrangements during MOF growth by considering other upgrades of nickel-based MOFs, such as metal doping [83] and the incorporation of MWCNTs [84]. They employed  $\text{NiO/NF}$  as a sacrificial template and precursor to fabricate a well-aligned porous  $\text{NiO}@\text{Ni-BTC/NF}$  cylindrical cage structure. The nickel foam (NF) substrate facilitated electron conductivity and surface area, while the exposed nickel ions' active sites acted as connecting joints for further MOF growth. The composite exhibited an exceptional specific capacity of  $1853 \text{ C cm}^{-2}$  at  $1 \text{ mA cm}^{-2}$ , much surpassing that of  $\text{NiO/NF}$ , which is  $242 \text{ C cm}^{-2}$ . The hybrid supercapacitor with carbon nanotubes as the negative electrode exhibited a specific capacitance of  $144 \text{ F g}^{-1}$  and maintained 94% capacity retention after 3000 cycles. Li et al. [85] similarly

produced NiO nanoparticles on hexagonal Ni-BTC using the calcination of the metal-organic framework (Figure 6). The TG analysis indicated the temperature at which weight loss commenced; hence, by regulating the calcination temperature at 350 °C, just a portion of the MOF converted to oxide. The distribution of NiO nanoparticles within the metal-organic framework not only enhanced electrolyte ion movement but also augmented the redox active sites. The composite electrode exhibited a better specific capacity (approximately 1100 F g<sup>-1</sup>) for 5000 cycles at 0.5 A g<sup>-1</sup>, in contrast to the non-modified MOF (approximately 900 F g<sup>-1</sup>) and the calcined variants at 450 °C (approximately 250 F g<sup>-1</sup>) and 550 °C (approximately 110 F g<sup>-1</sup>). Furthermore, the Ni-MOF@NiO//AC supercapacitor demonstrated a peak specific capacitance of 228.6 F g<sup>-1</sup> and an energy density of 62.2 Wh kg<sup>-1</sup>.

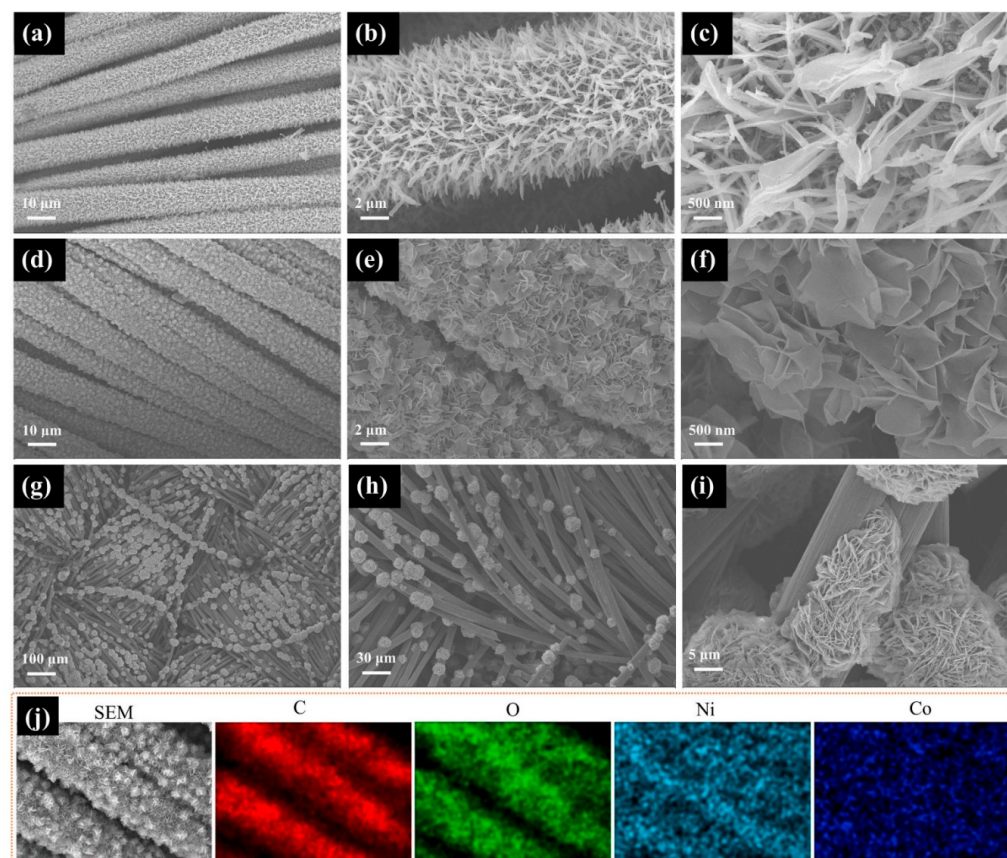


**Figure 5.** SEM images of ribbonlike Co<sub>3</sub>O<sub>4</sub> nanoarrays (a–c), Co<sub>3</sub>O<sub>4</sub>@Ni-MOF composites (d–f), Ni-MOF directly grown on carbon cloth (g–i), and EDX element mappings of Co<sub>3</sub>O<sub>4</sub>@Ni-MOF composites (j). (Reproduced from [76] with permission).

Efforts have been made to employ iron oxides among the many metal oxides utilized in SC composite electrodes. Notwithstanding their low costs and low toxicity, nanoparticles experience aggregation and elevated resistance, which constrains their electrochemical uses [86]. Chameh et al. [87] have synthesized iron oxide composites utilizing ZIF-8 and/or ZIF-67 through decoration using Fe<sub>2</sub>O<sub>3</sub> or applying a layer of ZIF onto Fe<sub>3</sub>O<sub>4</sub> to create a core-shell structure [88]. The ZIF-8 composite exhibited superior specific capacitance at 2.7 A g<sup>-1</sup> (1160 F g<sup>-1</sup>) compared to the ZIF-67 counterpart (573 F g<sup>-1</sup>), including at elevated current densities. Additionally, the ZIF-8/Fe<sub>2</sub>O<sub>3</sub>//AC supercapacitor achieved 28.5 Wh kg<sup>-1</sup> at 2.4 kW kg<sup>-1</sup>, with a 97% retention after 1500 cycles. Conversely, the synthesis of core-shell structures enhanced performance, resulting in ZIF-67 achieving 1334 F g<sup>-1</sup>, surpassing ZIF-8's 870 F g<sup>-1</sup> at 1 A g<sup>-1</sup>. The Fe<sub>3</sub>O<sub>4</sub>@ZIF-67//AC device

demonstrated  $27.9 \text{ Wh kg}^{-1}$  at  $5.49 \text{ kW kg}^{-1}$ , with an 87% retention over 3000 cycles. A magnetic  $\text{Fe}_2\text{O}_3@\text{SiO}_2$  core-shell structure was also synthesized using a solvothermal technique, with a Ni–BTC shell [89]. Upon evaluation as an electrode, it demonstrated a capacitance of  $600 \text{ F g}^{-1}$  at a current density of  $1.5 \text{ A g}^{-1}$  and exhibited a degradation of 5% following 1000 charge-discharge cycles.

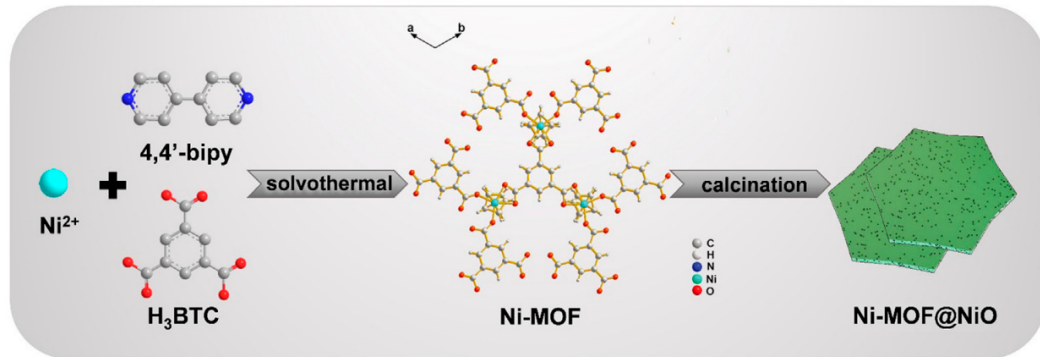


**Figure 6.** Schematic illustration of the preparation of Ni–MOF@NiO. (Reproduced from [85] with permission).

$\text{ZnO}$  has proven to be a compelling oxide in the fields of photocatalysis [90,91] and electrocatalysis [92,93]. The  $\text{ZnO}$  carbon composites have potential outcomes as semiconductor materials due to their thermal and chemical resilience, as well as their electronic conductivity [94]. Liu and coworkers [95] reported an electrode based on PANI/ $\text{ZnO}/\text{ZIF}-8/\text{graphene/polyester-textile}$  concerning MOF composites.  $\text{ZnO}$  was originally coated onto the graphene/polyester substrate and then served as a precursor for the *in situ* coating of ZIF-8, while PANI was electrochemically deposited. The electrode exhibited remarkable capacity ( $1378 \text{ F cm}^{-2}$  at  $1 \text{ mA cm}^{-2}$ ) by utilizing the internal ZIF surface area (Electric Double Layer Capacitance (EDLC)) and the PANI electron bridge (pseudocapacitance). The capacitance retention decreased to 73% after 400 cycles, likely due to the volume change of PANI during the charge-discharge process. Furthermore, the built flexible supercapacitor exhibited a commendable energy density of  $235 \text{ mWh cm}^{-3}$  at  $1542 \text{ mW cm}^{-3}$ . Zhu and colleagues have similarly utilized a carbon fabric substrate [96]. The alteration in CV cycles between 5 and 13 influenced the electrodeposition of PANI directly by increasing its thickness and was crucial to the end-product characteristics.

Electrochemical investigation confirmed the optimal performance achieved ( $340.7 \text{ F g}^{-1}$  at  $1 \text{ A g}^{-1}$  and 82.5% retention after 5000 cycles at  $2 \text{ A g}^{-1}$ ). Without ZIF-8 in the electrode, the retention decreased to 61.4%, underscoring its essential function in the composite. Zuhri et al. [97] enhanced the supercapacitive performance of a  $\text{ZnO-FC}$  (functionalized carbon) electrode by including a Ni–Co MOF derived from phthalic acid and pyrazine by a straightforward stirring-blending technique. The MOF implementation indeed enhanced the performance from 1.15 to 2.56 (10 wt%) and  $6.62 \text{ F g}^{-1}$  (20 wt%), although the results remained subpar in comparison to analogous materials.

$\text{TiO}_2$  has predominantly been investigated for solar and photocatalysis applications owing to its stability, low costs, and non-toxicity [98]. Ramasubbu et al. [99] synthesized a porous  $\text{TiO}_2$  aerogel/Co-MOF composite with 3D hierarchical structure by modifying a sol-gel method. Aerogels, characterized as porous materials, exhibit substantial specific surface areas, minimal density, and superior thermal conductivity [100,101]. The introduction of the MOF into the aerogel enhanced the electrode's specific capacity from  $66.4$  to  $111.2 \text{ C g}^{-1}$  at  $0.8 \text{ A g}^{-1}$  due to an increase in electroactive sites, a reduction in diffusion route length, and improved electron/ion transport. The constructed so-called supercapattery utilizing a

negative electrode based on activated carbon achieved a specific power of  $1875 \text{ W kg}^{-1}$  at a specific energy of  $0.4 \text{ Wh kg}^{-1}$ , with a remaining capacity of 93% after 5000 cycles.

Kitchametti et al. [102] recently presented a study on the application of a core–shell architecture comprising hierarchical 2D Manganese Dioxide ( $\text{MnO}_2$ ) nanoflakes and 1-D Nickel Titanate ( $\text{NiTiO}_3$ ) (NTO) mesoporous rods as a highly effective supercapacitor electrode, which offers a substantial surface area and enhanced pathways for  $\text{OH}^-$  ion diffusion. The hybrid porous core–shell hetero-architecture of  $\text{MnO}_2@\text{NTO}$ , processed through a two-step chemical method, achieves a specific capacitance of  $1054.7 \text{ F/g}$ , a specific power of  $11879.87 \text{ W/kg}$ , and a specific energy of  $36.23 \text{ Wh/kg}$ . Additionally, a retention of 85.3% in capacitance is observed after 5000 cycles, along with no degradation in the surface morphological characteristics.

## 2.2. MOFs@Sulfides

Metal sulfides are another intriguing material for supercapacitive performance. Numerous studies indicate that transition metal sulfides (TMS) are materials characterized by high conductivity and significant redox reactivity [103–106].

The synergistic interaction between MOFs and sulfides has been investigated in multiple facets of photocatalysis and electro-catalysis [107,108]. Lee et al. [109] reported the in situ synthesis of Ni–BDC on NF utilizing two distinct surfactants. The use of urea enhanced the structural density and thickness due to its functional groups interacting with the BDC linker. Conversely, PVA induced voids in the MOF nanoblocks, resulting in a 2D nano-sized harmonica-like morphology, likely because of the PVA- $\text{Ni}^{2+}$  complexation, which functioned as a structure-directing reagent. XRD data indicated that upon sulfurization, additional peaks emerged corresponding to  $\text{NiS}_2$  phases, but the primary MOF peaks persisted. The boundary section of the PVA sample was transformed into the  $\text{NiS}_2@\text{C}$  core, as confirmed by different analytical methods (XPS, SEM/EDS, TEM). The electrode exhibited the maximum specific capacitance of  $2780 \text{ F g}^{-1}$  at  $2 \text{ A g}^{-1}$ , maintaining 88% of its starting capacity after 10,000 cycles. The built flexible ASC, utilizing an activated carbon-supported negative electrode and PVA-KOH gel electrolyte, had a capacitance of  $283.5 \text{ F g}^{-1}$  with an energy density of  $77.2 \text{ Wh kg}^{-1}$  at  $7000 \text{ W kg}^{-1}$ . Zhang et al. [110] have synthesized Ni–BDC@ $\text{NiS}_2$  nanosheet arrays by initially growing Ni–BDC on a carbon cloth substrate and subsequently partially converting it to  $\text{NiS}_2$ . The ultrathin surface offered an extensive active area, resulting in excellent rate performance and specific capacitance ( $1128 \text{ F g}^{-1}$  at  $2 \text{ A g}^{-1}$ ), with the constructed Ni-MOF@ $\text{NiS}_2//\text{AC}$  supercapacitor retaining 95.2% capacity after 10,000 cycles.

Yue et al. [111] have documented a technique in which  $\text{MoS}_2$  nanoflowers were incorporated into the accordion-like Ni–BDC. In summary,  $\text{MoO}_4^{2-}$  infiltrated the MOF sheets, and sulfur facilitated the production of the composite, with the development of  $\text{NiS}$  corroborated by XRD and XPS analyses. The incorporation of nonmetals established a framework that enhanced the underpotential deposition sites, resulting in a specific capacitance three times greater ( $1590 \text{ F g}^{-1}$ ) than that of the pure MOF. The ASC  $\text{MoS}_2@\text{Ni-BDC} // \text{Activated-Carbon}$  exhibited an energy density of  $72.93 \text{ Wh kg}^{-1}$  at a power density of  $375 \text{ W kg}^{-1}$ , with a capacitance retention of 94.61% after 10,000 cycles.

Transition metal sulfides (TMSs) are currently being considered as appropriate materials for HSC positive electrodes because of the theoretically expected elevated capacity and electrochemical reactivity [103,112,113]. However, during participation in redox reactions, their crystalline phase structures experience irreversible alterations, resulting in structural collapse [114], which diminishes material stability, reduces electrical conductivity, and hinders advancements in electrode materials. A proficient strategy to tackle this issue involves the integration of TMSs with materials that possess structural integrity, exten-

sive pore architectures, and elevated electrical conductivity, such as carbon, employing particular methodologies [115].

### 2.3. MOF-Based Composites

Due to their intrinsic features, metal–organic frameworks (MOFs) have been extensively utilized as templates for the synthesis of carbons, oxides, chalcogenides, or hybrids [116]. Cobalt oxide is highly esteemed in the electrochemical field due to its catalytic activity, substantial theoretical capacity, various crystal dimensions, valence states, and low price [117]. ZIF-67, being one of the most extensively researched metal–organic frameworks (MOFs), has frequently been employed by numerous researchers as a cobalt-based template for the synthesis of  $\text{Co}_3\text{O}_4$  [118,119].

Recently, Kitchamsetti and Kim [120] have prepared a hierarchical FeCo-MIL-88 (FC-MOF) derived  $\text{CoFe}_2\text{O}_4$  and  $\text{NiMn}_2\text{O}_4$  (CFO@NMO) composite through a hydrothermal method. The hybrid CFO@NMO electrode demonstrated a remarkable specific capacity of  $353.6 \text{ mAhg}^{-1}$ , along with an impressive capacity retention of 86.1% after 5000 cycles. A hybrid supercapacitor (HSC) device was constructed to utilize the advantages of extremely high cycling stability and specific capacity, employing AC/NF (Nickel foam (NF), activated carbon (AC)) for the negative electrode and CFO@NMO / NF for the positive electrode, both utilizing an aqueous electrolyte. The constructed hybrid supercapacitor device presented a specific capacitance of  $312.8 \text{ Fg}^{-1}$ , demonstrating an impressive 88.4% retention in capacitance after 10,000 GCD cycles, alongside a notable energy density of  $90.3 \text{ Whkg}^{-1}$  and power density of  $12.9 \text{ kWkg}^{-1}$ .

Recent works combine metal–organic frameworks with transition metal nitrides like chromium nitride interfacial layers for the preparation of hybrid supercapacitors with high efficiency. A hybrid supercapacitor based on a two-cell mode was developed utilizing activated carbon and chromium nitride/copper-trimesic acid. The results showed an impressive energy density of  $94.5 \text{ Whkg}^{-1}$  and a maximum power density of  $7750 \text{ Wkg}^{-1}$ , operating at 1.6 V, with a cycling stability of 97.9% after 3000 galvanostatic charge-discharge cycles [121].

### 2.4. MOFs@Oxides/Sulfides

Wang and colleagues [122] synthesized a  $\text{Co}_3\text{O}_4/\text{C}@\text{MoS}_2$  core-shell structure using a double thermal treatment of ZIF-67 followed by solvothermal addition of  $\text{MoS}_2$ . The comparative analysis of cycling stability for the composite (specific capacitance of  $1076 \text{ F g}^{-1}$  at  $1 \text{ A g}^{-1}$ ),  $\text{Co}_3\text{O}_4/\text{C}$ , and  $\text{MoS}_2$  demonstrated superior performance, with retention rates of 64.5%, 60.6%, and 50.5% over 5000 cycles at  $10 \text{ A g}^{-1}$ , respectively. The  $\text{MoS}_2$  content significantly influences electrochemical behavior; a low quantity (10 mg of Mo precursor) restricts electron and ion transfer, while a higher quantity (30 mg) impedes diffusion, making an average of 20 mg the optimal loading. A further treatment of ZIF-67 involved a chemical conversion to  $\text{Co}_3\text{S}_4$  using thioacetamide at  $120^\circ\text{C}$ , followed by the NiO deposition on it to produce  $\text{Co}_3\text{S}_4@\text{NiO}$  hollow dodecahedrons [123]. The resulting architecture facilitates a more concise electron pathway, while the NiO outer layer enhances surface area and active sites. The augmentation of sulfide is demonstrated by the specific capacitance, which rises from 1416 to  $1878 \text{ F g}^{-1}$  at  $1 \text{ A g}^{-1}$  upon the addition of NiO. The composite electrode was assessed within an asymmetric supercapacitor (ASC) utilizing activated carbon as the negative electrode, achieving a capacitance of  $164.8 \text{ F g}^{-1}$  at  $1 \text{ A g}^{-1}$  and  $115 \text{ F g}^{-1}$  over 10,000 cycles at  $5 \text{ A g}^{-1}$ , with a retention rate of 86.1%. Zhao et al. [124] have synthesized ZIF materials in order to use them as templates for both negative and positive electrodes of an ASC developed on flexible CNT fibers. The CNTFs@ $\text{ZnCo}_2\text{O}_4@\text{Zn-Co-S}$  positive electrode was synthesized through the processes of annealing and sulfurization of  $\text{Zn}/\text{Co}$ .

ZIF, whereas the CNTFs@H<sub>Co<sub>3</sub>O<sub>4</sub></sub>@CoNC negative electrode was obtained from Co-ZIF (ZIF-67) via oxidation and pyrolytic processes. SEM micrographs and characterization data of the prepared CNTFs are illustrated in Figure 7.

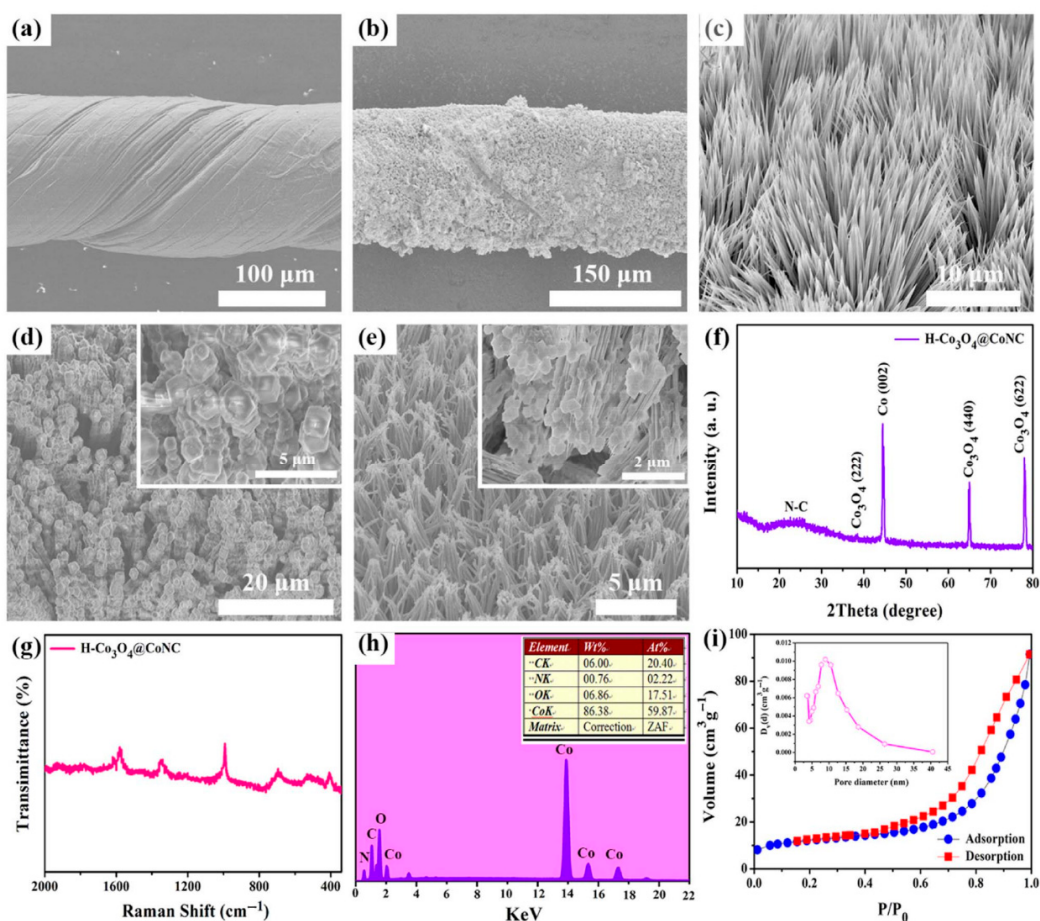


**Figure 7.** (a) SEM images of CNTFs. (b) Low- and (c) high-magnification SEM images of CNTFs@H-Co<sub>3</sub>O<sub>4</sub> NA. (d) SEM images of as-prepared CNTFs@H-Co<sub>3</sub>O<sub>4</sub>@ZIF-67 HA. Inset: enlarged SEM image. (e) SEM images of as-prepared CNTFs@H-Co<sub>3</sub>O<sub>4</sub>@CoNC HA. Inset: enlarged SEM image. (f) Powder XRD patterns of as-prepared CNTFs@H-Co<sub>3</sub>O<sub>4</sub>@CoNC HA. (g) Raman spectra of as-prepared CNTFs@H-Co<sub>3</sub>O<sub>4</sub>@CoNC HA. (h) EDS of the as-prepared samples. (i) N<sub>2</sub> adsorption/desorption isotherms of the as-prepared CNTFs@H-Co<sub>3</sub>O<sub>4</sub>@CoNC HA. Inset image shows the pore size distribution. (Reproduced from [124] with permission).

The integration of the ASC in triboelectric nanogenerators for energy harvesting and self-charging, presenting a prospective use in wearable electronics, is very interesting. The investigation of both flexibility and mechanical stability involved the selection of diverse bending angles, resulting in a retention rate of 93.9% after 5000 cycles (Figure 8). The constructed gadget demonstrated a significant areal energy density of 32 mWh cm<sup>-2</sup> at a power density of 698 mW cm<sup>-2</sup>.

Recently, ZIF-67 was cultivated on Cu<sub>x</sub>O nanowires, which were subsequently annealed to form Cu<sub>x</sub>ONWs@Co<sub>3</sub>O<sub>4</sub> and then sulfurized to produce Cu<sub>x</sub>ONWs@CoS<sub>2</sub> [125]. TEM images demonstrate that the NWs penetrate the hollow Co<sub>3</sub>O<sub>4</sub> rhombic dodecahedrons, ensuring mechanical integrity and facilitating electron transport channels. The oxide and sulfide composites were analyzed over 10,000 cycles, achieving retention rates of 112.3% and 100.2%, respectively, attributed to a substantial number of electroactive sites. An uncommon metal selection was utilized with Ce-BTC as the template for CeO<sub>2</sub>/C/MoS<sub>2</sub> [126]. The hybrid electrode is more efficient compared to both MoS<sub>2</sub> (300 F g<sup>-1</sup>) and CeO<sub>2</sub>/C

( $727 \text{ F g}^{-1}$ ), achieving a specific capacitance of  $1326 \text{ F g}^{-1}$  at  $1 \text{ A g}^{-1}$  and maintaining 92.8% capacity after 1000 cycles. The performance is ascribed to carbon conductivity, 2D MoS<sub>2</sub> nanosheets, and the elevated surface area of CeO<sub>2</sub>. Furthermore, the ASC exhibited commendable stability across an equivalent number of cycles, alongside a high energy density ( $34.5 \text{ Wh kg}^{-1}$ ) at  $667 \text{ W kg}^{-1}$ .

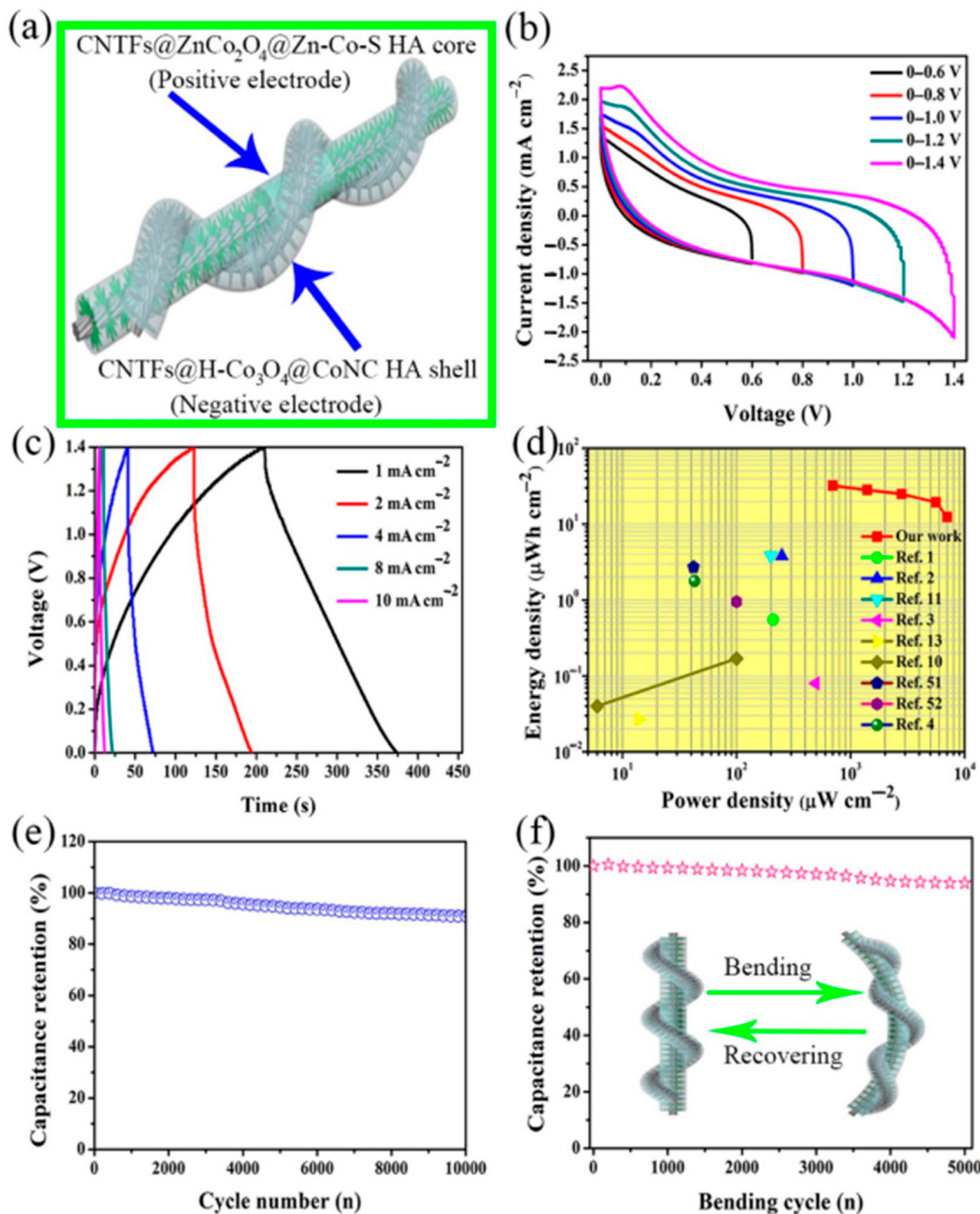


**Figure 8.** The assembled FASC device. (a) Schematic of the assembled structure of the FASC. (b) CV of the assembled device measured for different voltage windows. (c) GCD curves of the assembled flexible asymmetric supercapacitor (FASC) at different current densities. (d) Ragone plot (power density vs. energy density) of the FASC device. (e) Cyclic stability. (f) Capacitance retention after 5000 cycles of bending. (Reproduced from [124] with permission).

## 2.5. MOFs@Oxides/Phosphides

Recently, CoP<sub>x</sub>/CoO composites using the calcination of 2D ZIF-67, followed by partial phosphidation using varying phosphorus concentrations, have been synthesized according to the procedure illustrated in Figure 9 [127]. Hybrids are also documented in OER catalysis [128] and Na–O<sub>2</sub> batteries [129]. The combination of phosphides' redox

activity and oxides' stability led to improved supercapacitor performance [127]. XRD examination and Rietveld refinement demonstrated that increasing the phosphorus content results in the predominance of phosphide phases ( $\text{CoP}$ ,  $\text{Co}_2\text{P}$ ) over  $\text{CoO}$  in the composite. Despite utilizing a substantial quantity of phosphorus, the oxide did not achieve complete transformation; the augmentation of phosphorus content from 40 wt% to 100 wt% resulted in merely a 4% improvement from  $(\text{CoP}_x)_{0.90}/\text{CoO}_{0.10}$  to  $(\text{CoP}_x)_{0.94}/\text{CoO}_{0.06}$ , attributed to the initial stability of ZIF, which was maintained in the  $\text{Co}_3\text{O}_4$  phase, inhibiting the diffusion of the produced  $\text{PH}_3$  gas into the bulk. Nonetheless, the  $\text{Co}_2\text{O}_3$  could not be retained in the final composite due to the potent reducing nature of  $\text{PH}_3$ .  $(\text{CoP}_x)_{0.90}/\text{CoO}_{0.10}$  exhibited a specific capacitance of  $467 \text{ F g}^{-1}$  at  $5 \text{ A g}^{-1}$  and maintained 91% retention over 10,000 cycles at  $30 \text{ A g}^{-1}$ , while the equivalent material with rGO demonstrated comparable specific capacitance and 107% retention.

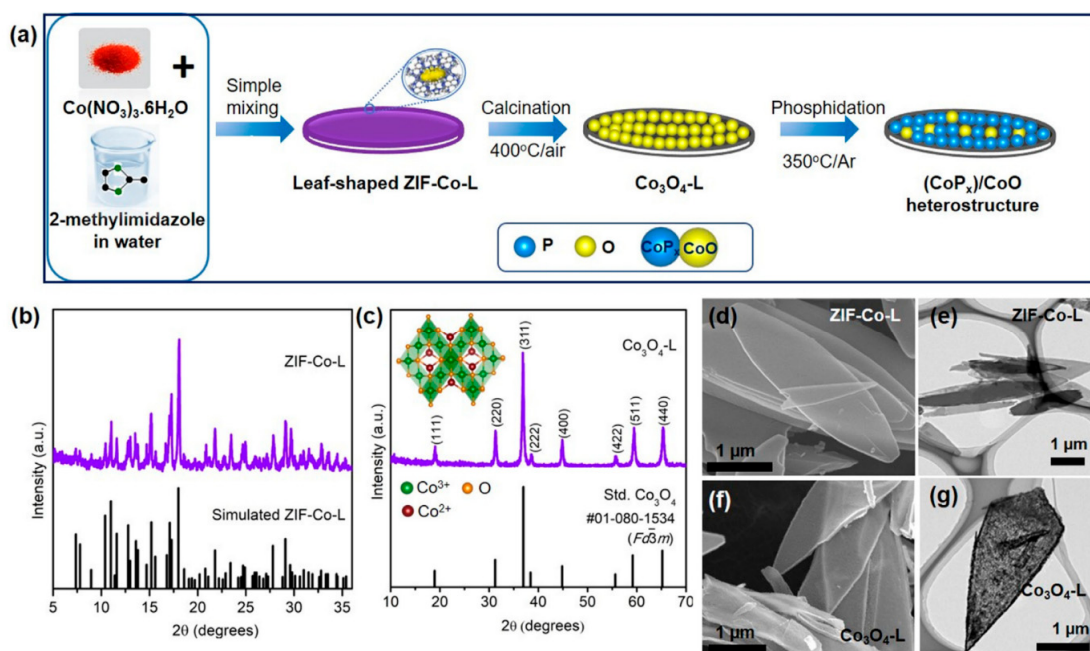


**Figure 9.** Synthesis scheme of leaf-shaped  $\text{CoP}_x/\text{CoO}$  heterostructure and structural analysis of precursor. (a) Scheme for the synthesis of  $\text{CoP}_x/\text{CoO}$  heterostructure; Powder XRD of (b) ZIF-Co-L and (c)  $\text{Co}_3\text{O}_4$ -L precursors; (d) SEM and (e) TEM of ZIF-Co-L precursor; (f) SEM and (g) TEM images of  $\text{Co}_3\text{O}_4$ -L precursor. (Reproduced from [127] with permission).

## 2.6. Other Composite Combinations

Guo and coworkers [130] have prepared metal nitride-based 3-D stacked hierarchical  $\text{Ni}_3\text{N}-\text{CoN}/\text{NC}$  nanosheets for flexible and freestanding supercapacitor electrodes with remarkable energy density of  $0.2144 \text{ mWh cm}^{-2}$  and a peak power density of  $80 \text{ mW cm}^{-2}$ , demonstrating remarkable cycling stability of 92.3% after 15,000 cycles.

Zhao et al. [131] have recently synthesized amorphous spherical carbon materials featuring hierarchical pores (DHTAC-2) through a one-step carbonization process of Al-MOF. The carbon exhibits a significant specific surface area of  $2666 \text{ m}^2 \text{ g}^{-1}$  and a considerable pore volume of  $2.35 \text{ cm}^3 \text{ g}^{-1}$ . The carbon obtained (DHTAC-2) shows a remarkable specific capacitance of  $298.8 \text{ F g}^{-1}$  at a current density of  $1 \text{ A g}^{-1}$ , along with impressive capacitance retentions of 97.3% and 98.0% after 120,000 cycles at current densities of  $50 \text{ A g}^{-1}$  and  $100 \text{ A g}^{-1}$ , respectively. Furthermore, the Nitrogen-doped carbon (N-DHTAC) exhibits an elevated presence of pyridine-N, pyrrole-N, and graphite-N content. The three types of N led to notable enhancements in wettability, reversible pseudocapacitance, and conductivity, culminating in an impressive capacitance of  $355.0 \text{ F g}^{-1}$  at  $1 \text{ A g}^{-1}$  and an increased energy

density of  $17.7 \text{ Wh kg}^{-1}$  at  $350 \text{ W kg}^{-1}$  for the assembled electric double-layer capacitor (EDLC) device.

Zhang et al. [132] produced a series of chalcogenides generated from ZIF-67 on cotton fabric, which was further subjected to thermal treatment under various conditions along with chalcogenide powders to obtain CF@CoX (X = O, S, Se, Te). The flakes were uniformly deposited onto the carbon fibers, creating a three-dimensional hierarchical structure. Of the four synthesized electrodes, the sulfide exhibited the highest areal specific capacity ( $3.58 \text{ F cm}^{-2}$ ) at  $5 \text{ mA cm}^{-2}$ , followed by the selenide ( $2.43 \text{ F cm}^{-2}$ ), the telluride ( $1.8 \text{ F cm}^{-2}$ ), and the oxide ( $0.67 \text{ F cm}^{-2}$ ). CF@CoS demonstrated superior performance relative to other components in the ASC device, utilizing an AC cloth (made through a process akin to cotton pyrolysis) as the negative electrode, achieving  $0.77 \text{ F cm}^{-2}$  and an energy density of  $149 \text{ mWh cm}^{-2}$  at  $4.3 \text{ mW cm}^{-2}$ .

Zhang et al. [133] summarize, in a recent work, advancements in the field of multi-dimensional MOF-based materials and their derivatives across various dimensionalities, encompassing 1-D nanopowders, 2-D nanofilms, 3-D aerogels, and 4-D self-supporting electrodes for supercapacitors. Additionally, the primary challenges and viewpoints regarding MOFs and their derivative materials for practical and sustainable electrochemical energy conversion and storage applications are succinctly addressed, potentially serving as a framework for the design of next-generation electrode materials across various dimensionalities.

### 2.6.1. MOFs/Graphene

Graphene and graphene-like materials have gained significant interest because of their high electrical conductivity, superior power density, and stable chemical properties. The exploration of nanostructures has been extensive in various fields, including energy storage [134,135]. Metal–organic frameworks have been utilized in energy systems; however, they exhibit low conductivity and stability challenges in practical applications [136].

A recent study of Saxena et al. [137] presents the preparation of a rGO/Ppy/Zn-MOF ternary composite using graphene oxide, pyrrole, and a zinc metal–organic framework precursor, specifically  $\text{Zn}(\text{NO}_3)_2 \cdot 6\text{H}_2\text{O}$  and imidazole, through a straightforward hydrothermal one-pot method. The synthesized rGO/Ppy/Zn-MOF composite demonstrated exceptional electrochemical properties. In energy storage applications, the synthesized rGO/Ppy/Zn-MOF demonstrated remarkable specific capacitance of  $175 \text{ F g}^{-1}$  at a current density of  $1 \text{ A g}^{-1}$ , a specific energy of  $19.68 \text{ Wh kg}^{-1}$ , and a specific power of  $1792 \text{ W kg}^{-1}$ . Exhibiting cyclic stability at  $10 \text{ A g}^{-1}$ , it maintains up to 82% of its starting capacitance even after more than 7000 repetitive cycles.

In order to further increase the active surface graphene, aerogels have also been employed. Graphene has been utilized in methodological energy strategies owing to its remarkable structure and characteristics; however, its application is constrained by issues related to nanosheet aggregation [136]. The development of nitrogen-doped graphene aerogel (N-GA) featuring a three-dimensional structure can significantly inhibit the stacking and aggregation of graphene flakes while preserving the benefits of electrical conductivity [138]. In this respect,  $\text{MoS}_2$  derived from MOFs with a mixed 1T/2H phase was synthesized using a straightforward one-step hydrothermal method, and the assembly of MOFs-derived  $\text{MoS}_2$  with nitrogen-doped graphene aerogel (N-GA) resulted in the formation of  $\text{MoS}_2/\text{N-GA}$ . The findings indicated that employing N-GA as the carrier for MOFs-derived  $\text{MoS}_2$  not only improved the electrical conductivity of the composites but also mitigated the volume expansion and contraction of  $\text{MoS}_2$  during the charging and discharging processes, attributed to its distinctive three-dimensional structure. The capacitive performance of MNGA20 (20% N-GA) outperformed that of MNGA10 (10% N-GA) and MNGA30 (30% N-GA). MNGA20 composites demonstrated the lowest charge transfer resistance and achieved an

optimal specific capacitance of  $530 \text{ F g}^{-1}$  at  $1 \text{ A g}^{-1}$ , maintaining 80.2% capacitance after 1000 charge-discharge cycles at  $10 \text{ A g}^{-1}$  [139].

Trimesic acid-based MOFs are often the choice for the preparation of composites with graphene materials [140]. Other MOFs used in similar composites with graphene are based on imidazolate [141,142], zirconium [143], as well as terephthalic acid [144].

### 2.6.2. MOFs/Phosphides

Transition metal phosphides (TMPs) exhibit high electrical conductivity and remarkable physicochemical properties, demonstrating significant potential for enhancing the capacitance and energy density of supercapacitors [145]. MOF-derived dual phosphide composites are rare as supercapacitor electrodes in the development of phosphide materials. Conversely, MOF-derived carbon/phosphide hybrid materials have been utilized in several applications in recent years [146].

Zhou et al. [147] synthesized NiCoP/C nanohybrids with varying ratios, that involve monometallic phosphides, contingent upon the initial concentration during the production of the metal–organic framework utilizing a phenanthroline linker. The annealing of the MOF occurred in a nitrogen environment, leading to the anchoring of NiCoP nanoparticles onto the carbon. The composite exhibited a notable specific capacity of  $775.7 \text{ C g}^{-1}$  at  $1 \text{ A g}^{-1}$  and  $582.4 \text{ C g}^{-1}$  at  $20 \text{ A g}^{-1}$ , while the completed supercapacitor provided  $47.6 \text{ Wh kg}^{-1}$  at  $799 \text{ W kg}^{-1}$ . Liu and coworkers [148] have prepared nickel phosphide and nickel cobalt phosphide heterostructure nanocomposites (NP@NCP) synthesized through the phosphidization of metal–organic framework (MOF) precursors leading to a morphology with nanosheets hierarchically arranged to form microflower-like particles. The NP@NCP exhibit a morphology like that of MOF, yet they possess a significantly higher porosity. The NP@NCP31 material on carbon cloth, when utilized as the electrode material, demonstrates a specific capacity of  $868.1 \text{ C g}^{-1}$  at  $1 \text{ A g}^{-1}$ , with 82.05% of its capacity retained after 5000 cycles in 4 M KOH. An asymmetric supercapacitor made with NP@NCP31 and activated carbon demonstrates an energy density of  $61.9 \text{ Wh kg}^{-1}$  at a power density of  $800.1 \text{ W kg}^{-1}$ , along with a capacity retention rate of 94.17% after 5000 cycles. The impressive charge-storage performance of the NP@NCP is attributed by the authors to the development of a heterointerface, which induces charge redistribution, enhances the number of electrochemically active sites, and promotes ion diffusion.

A different viable synthetic method has been investigated involving the use of an ionic liquid (IL) in the synthesis of MOFs. Although ionic liquids (ILs) are primarily utilized as substitutes for organic solvents, their incorporation into DMF was essential for nitrogen and phosphorus doping, as well as for the introduction of a different morphology with wrinkles and folds resulting from partial collapse during the following carbonization and phosphorization processes under argon/hydrogen flow, ultimately yielding the NiCoP/NPC composite [149]. Additionally, the scientists noted applying this procedure results to a five times higher surface area, while the constructed ASC demonstrated  $40.2 \text{ Wh kg}^{-1}$  at a power density of  $800.2 \text{ W kg}^{-1}$ . Similar electrode materials based on C/NiCoP have been recently developed and tested. The prepared C/NiCoP material exhibits a flower-like structure with specific capacitance of  $773 \text{ C g}^{-1}$  at  $1 \text{ A g}^{-1}$  [150].

Bimetallic phosphides based on nickel and manganese have been synthesized through the phosphidization of bimetallic hydroxides derived from metal–organic frameworks. The bimetallic phosphides consist of nanosheets and display a crystalline  $\text{Ni}_2\text{P}$  phase, with a high specific surface area. When utilized on carbon cloth (CC) and employed as the electrode material in 4 M KOH, the  $(\text{Ni}_{0.93}\text{Mn}_{0.07})_2\text{P-18}/\text{CC}$  exhibits a specific capacitance of  $851.1 \text{ C g}^{-1}$  at  $1 \text{ A g}^{-1}$  and retains 84.87% capacity following 5000 cycles. The investigation explores the origin of the high specific capacity, pointing out the electron interactions

between Mn and Ni sites, the elevated specific surface area, and the ease of ion transport, all of which contribute to the remarkable specific capacity and stability observed [151]. For Cu/Co phosphides density-functional theory (DFT) computations demonstrate that the Cu<sub>3</sub>P/CoP heterostructures enhance the metallic conductivity of the composite, exhibiting an increased density of electron-occupied states near the Fermi level and improving the charge-transfer efficiency of the heterostructure. The findings indicate that the Cu<sub>3</sub>P/CoP-1 composite, possessing a 1:1 Cu/Co molar ratio, has superior electrochemical performance. At a current density of 1 A g<sup>-1</sup>, a remarkable specific capacitance of 804.3 F g<sup>-1</sup> has been demonstrated, and when the current density is elevated to 10 A g<sup>-1</sup>, it maintains 92.8% of its capacitance over 10,000 cycles [152].

### 2.6.3. MOFs-Sulfides

The facile agglomeration of transition metal sulfides leads to a diminished specific surface area and sluggish reaction kinetics, resulting in volumetric expansion that compromises structural integrity and diminishes performance during prolonged electrochemical processes. To address these deficiencies, a preferred strategy is to develop a stable composite structure with rapid charge transfer capabilities. Numerous researchers have integrated metal sulfides generated from MOFs with preferably one-dimensional conductive materials to establish a stable structure. A new composite of nanoscale one-dimensional (1D) MXene fibers infused with metal sulfides produced from MOFs ( $\text{Ni}(\text{Co})_3\text{S}_4@\text{MXene-fibers}$ ) has been created (Figure 10). The electrochemical investigation indicates that the specific capacitance of  $\text{Ni}(\text{Co})_3\text{S}_4@\text{MXene-fibers}$  attains 829.4 C g<sup>-1</sup> at a current density of 1 A g<sup>-1</sup>. Furthermore, the asymmetric device ( $\text{Ni}(\text{Co})_3\text{S}_4@\text{MXene-fibers} // \text{AC}$ ) exhibits an energy density of 63.3 Wh kg<sup>-1</sup> at a power density of 850 W kg<sup>-1</sup> [153].

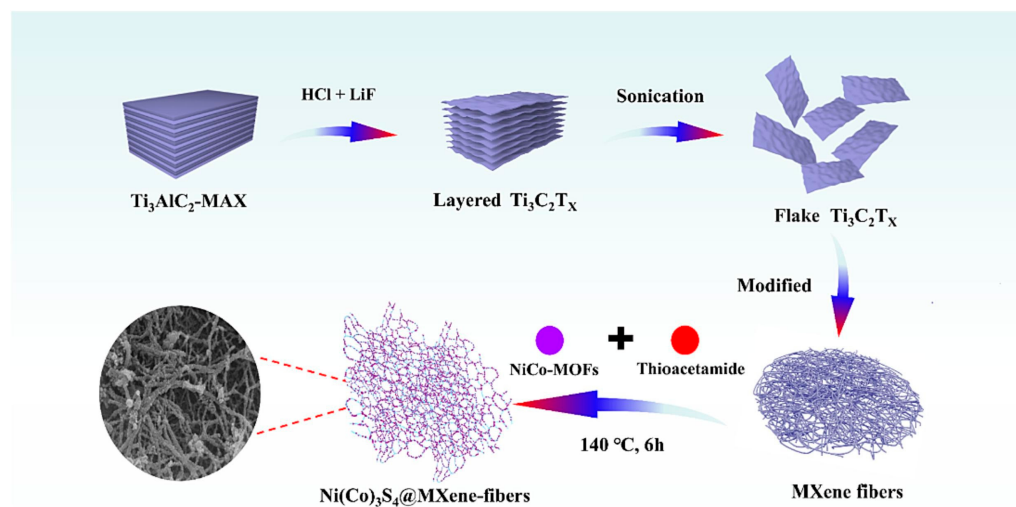


**Figure 10.** Schematic diagram of the synthesis of  $\text{Ni}(\text{Co})_3\text{S}_4@\text{MXene-fibers}$ . (Reproduced from [153] with permission).

Mono as well as bimetallic sulfides have proven to be viable materials due to simple fabrication techniques for energy applications [154–156]. Notably,  $\text{NiCo}_2\text{S}_4$  has been thoroughly investigated due to its exceptional electrochemical performance, resulting to the emergence of MOF-derived variants in literature as well [154,157–159]. Regarding sulfide composites, Li et al. [160] synthesized amorphous Ni/Zn-BDC spheres, which were then converted into  $\text{NiS}_2/\text{ZnS}$ . The reaction duration in the autoclave at 160 °C influences the diffusion of  $\text{S}^{2-}$  ions, resulting in the formation of core-shell structures (1 h), yolk-shell structures (3 h), and hollow spheres (6 h), as confirmed by SEM/TEM examination. The hollow spheres demonstrated commendable capacitance (1198 F g<sup>-1</sup> at 1 A g<sup>-1</sup>) relative to

other analogous nickel sulfide materials [161,162], which can be ascribed to the synergy between  $\text{NiS}_2$  and  $\text{ZnS}$ , enhancing ion/electron transfer, as well as the reduction in diffusion path owing to the mesoporous architecture. The  $\text{NiS}_2/\text{ZnS}/\text{AC}$  ASC exhibited a specific capacitance of  $89.7 \text{ F g}^{-1}$  at  $1 \text{ A g}^{-1}$ , with a retention rate of 88.7% after 1500 cycles.

Shrivastav and colleagues synthesized  $\text{Co}_3\text{S}_4/\text{WS}_2$  utilizing a ZIF-67 template [163]. The hollow  $\text{Co}_3\text{S}_4$  microspheres were solvothermally modified with 2D  $\text{WS}_2$  nanorods to improve energy density and facilitate ion/electron transfer. The electrode exhibited a capacitance of  $412.7 \text{ F g}^{-1}$  at a current density of  $1 \text{ A g}^{-1}$  and was utilized in a symmetrical supercapacitor with a broad potential window of 2 V, demonstrating 92% stability over 2000 cycles. Zhao et al. [164] created a flower-like trimetallic sulfide composite (Figure 11), referred to as  $\text{Cu}(\text{NiCo})_2\text{S}_4/\text{Ni}_3\text{S}_4$ . The combination exhibited a specific capacitance of  $1320 \text{ F g}^{-1}$  ( $1 \text{ A g}^{-1}$ ), in direct comparison to the  $\text{CuNiCo-OH}$  intermediate product, which measured  $670 \text{ F g}^{-1}$ . Furthermore, the  $\text{Cu}(\text{NiCo})_2\text{S}_4/\text{Ni}_3\text{S}_4/\text{AC}$  supercapacitor exhibited satisfactory cycling stability (85% retention) and achieved a maximum energy density of  $40.8 \text{ Wh kg}^{-1}$ , with a power density of  $7859 \text{ W kg}^{-1}$ .

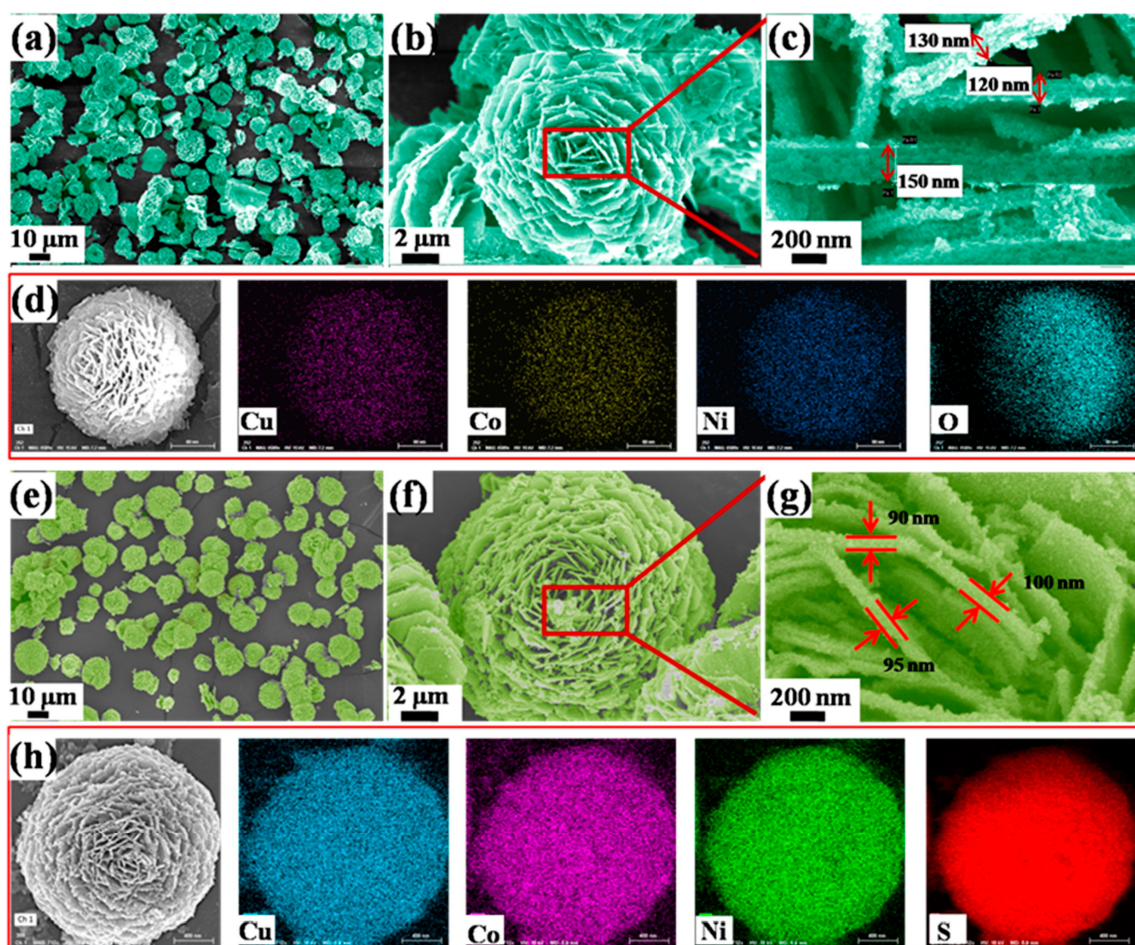


**Figure 11.** (a–c) SEM images of CoCuNi-OH and (d) the corresponding elemental mapping; (e–g) SEM images of  $\text{Cu}(\text{NiCo})_2\text{S}_4/\text{Ni}_3\text{S}_4$  and (h) the corresponding elemental mapping images. (Reproduced from [164] with permission).

Recently, Li et al. [165] have prepared flower like Co/Ni-MOFs (ZIF-67@Ni-salicylate) for supercapacitor electrodes exhibiting exceptional performance such as high specific capacitance of  $1493 \text{ F g}^{-1}$  at  $1 \text{ A g}^{-1}$  and at the same time excellent cycle stability. Xiong et al. [166] also synthesized bimetallic MOFs on Ni foam with two distinct techniques. The one-pot method utilized two metal precursors (Ni-Fe or Ni-Co) concurrently, whereas the two-

step synthesis (MOF-on-MOF) introduced the second metal precursor in the subsequent phase, following the formation of the initial MOF. The synergistic interaction between the two metals imparts enhanced efficiency to bimetallic catalysts in electrocatalysis, attributed to the enrichment of redox sites. Notably, FeMOF/NiMOF/NF exhibited exceptional performance, demonstrating modest overpotentials of 293 mV at 50 mA cm<sup>-2</sup> and 359 mV at 100 mA cm<sup>-2</sup>, along with commendable cycling stability, positioning it as an optimal candidate for OER catalysis. Additionally, it exhibited an areal capacitance of 1166 mF cm<sup>-2</sup> at a current density of 1 mA cm<sup>-2</sup>. A sulfurization method was conducted to investigate the sulfides in an ASC (with AC as the negative electrode), revealing that NiCoS/NF demonstrated a high specific capacitance of 2815.4 F g<sup>-1</sup> at 1 mA cm<sup>-2</sup>.

#### 2.6.4. MOFs–Selenides

In addition to sulfides, selenides are effective alternatives in hybrid semiconductor devices, exhibiting superior conductivity ( $1 \times 10^{-3}$  S m<sup>-1</sup>) and metallic characteristics compared to sulfur ( $5 \times 10^{-28}$  S m<sup>-1</sup>) [167–170]. Zhang et al. [171] synthesized nitrogen-doped cobalt selenides–carbon composites utilizing ZIF-67. By altering the treatment temperature, they generated distinct structures, e.g., a solid structure at 300 °C, a yolk-shell at 450 °C, and a double-shell at 600 °C. Mei et al. [172] also emphasized the importance of the structure during the synthesis of the MOF (Ni-BTC). As the reaction time extended (T = 150 °C), Ostwald ripening let the inner sphere progressively dissolve while the outer shell expanded, ultimately resulting in a hollow structure. After 10 h, a yolk-shell (730 C g<sup>-1</sup> at 2 A g<sup>-1</sup>) was obtained, whereas after 15 h, a hollow sphere (~600 C g<sup>-1</sup> at 2 A g<sup>-1</sup>) was ultimately formed. Additional carbon composites, including Co [173], Cu-Co [174], or Ni-Co [175], have also been examined as supercapacitor electrodes. Hollow and porous nickel–zinc–cobalt selenide (Ni–Zn–Co–Se) nanosheet configurations were, for the first time, synthesized on chemically reduced rGO-coated nickel foam (rGO/NF), utilizing a Zn–Co-organic framework as a template. The Ni–Zn–Co–Se@rGO/NF electrode, benefiting from its distinctive porous and hollow nanoarchitecture, offers numerous electroactive sites, extensive accessible areas for efficient electrolyte insertion, and reduced ion diffusion pathways, demonstrating outstanding electrochemical properties, including a specific capacity of 464.4 mA h g<sup>-1</sup>, a rate performance of 68.9%, and a remarkable cyclic lifespan of 93.24% after 7000 cycles in a three-electrode assembly for supercapacitors. An asymmetric supercapacitor (ASC) device was constructed (Figure 12) utilizing Ni–Zn–Co–Se@rGO/NF as the positive electrode and MOF-derived hollow porous carbon (MDHPC) as the negative electrode to illustrate its practical applicability. The obtained Ni–Zn–Co–Se@rGO/NF // MDHPC device demonstrated an energy density of 74.6 Wh kg<sup>-1</sup> at a power density of 796.91 W kg<sup>-1</sup>, along with an impressive durability of 96.4% after 7000 consecutive charge–discharge cycles [176].

A recent study by Dong and coworkers [177] centers on the advancement of multi-metal selenides (MMSes) that utilize synergistic effects to improve electrochemical performance by exploiting plentiful active sites and redox reactions. The metal–organic framework ZIF-67 is used as a morphological template by cultivating ZIF-67 on a NiMoO<sub>4</sub>·xH<sub>2</sub>O substrate. Subsequently it was selenized, leading to synthesis of a multi-metal selenide electrode material abundant in Ni, Co, and Mo, comprising NiSe, Ni<sub>3</sub>Se<sub>2</sub>, CoSe, and MoSe<sub>2</sub> phases. This electrode demonstrated a specific capacitance of 15.49 F cm<sup>-2</sup> at a current density of 5 mA cm<sup>-2</sup> and retains 96.5% of its capacitance after 10,000 cycles. The constructed asymmetric supercapacitor demonstrated an areal energy density of 0.301 mWh cm<sup>-2</sup> and an areal power density of 4 mW cm<sup>-2</sup>, with a capacity retention of 95.6% after 10,000 cycles at a current density of 50 mA cm<sup>-2</sup>.

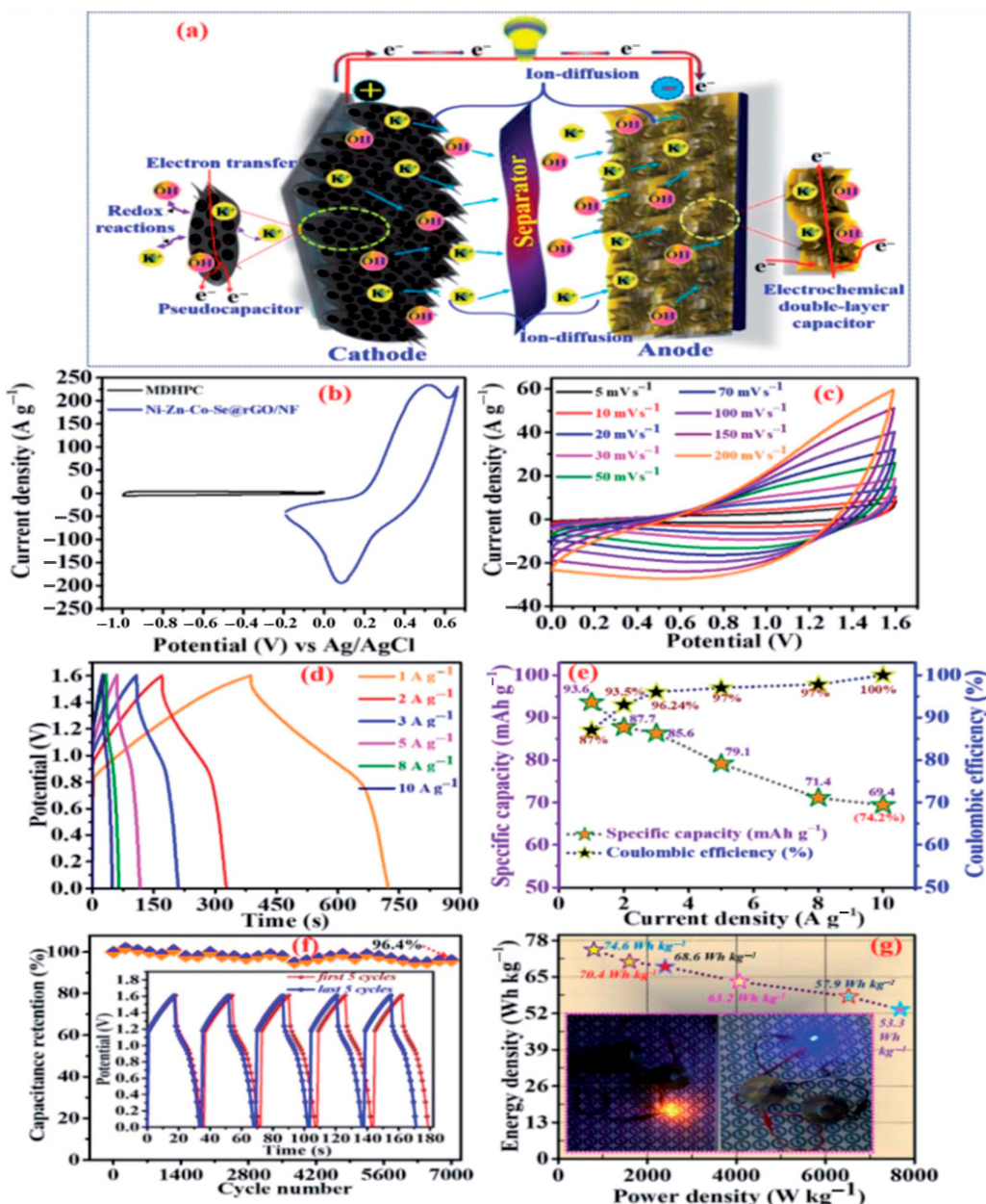


**Figure 12.** (a) Schematic diagram of the as-assembled ASC device, (b) CV curves of the cathode and anode within the respective potential of  $-0.2$  to  $0.7$  and  $-1$  to  $0$  V at a scan rate of  $20\text{ mV s}^{-1}$ , (c) CV curve of the ASC device at different scan rates of  $5$ – $200\text{ mV s}^{-1}$ , (d) GCD curves of the ASC device at different current densities of  $1$  to  $10\text{ A g}^{-1}$ , (e) specific capacity and coulombic efficiency at different current densities, (f) cyclic performance of the ASC device (inset figure shows the first and last five cycles), and (g) Ragone plot (inset shows the digital photograph of a yellow and blue LED bulb ignited with the help of the ASC device when connected in a series). (Reproduced from [176] with permission).

#### 2.6.5. MOFs–Sulfoselenides

Metal selenides are attractive materials for electrodes in advanced supercapacitors and energy harvesting applications [178]. Nonetheless, their performance remains constrained by inadequate utilization of active materials and the poor porosity of the electrodes. A potential solution to address these shortcomings is to manufacture composites using materials with inherent high porosity, such as MOFs.

A straightforward strategy is presented for the *in situ* synthesis of hierarchical mesoporous selenium@bimetallic selenide quadrilateral nanosheet arrays on diverse conduc-

tive substrates, utilizing two-dimensional bimetal porphyrin paddlewheel framework ( $MCo\text{-}TCPP$ , where TCPP denotes tetrakis(4-carboxyphenyl)porphyrin and M represents Ni or Zn) nanosheets as templates [179]. Yi et al. [180] produced a bimetallic metal–organic framework ( $NiCo\text{-BTC}$ ) for the production of a sulfoselenide. The MOF microspheres were annealed in an  $Ar/H_2$  environment to obtain  $NiCo_2$  on graphitic carbon (GC), which was further converted into  $NiCo_2(S_xSe_{1-x})_5$  nanoparticles confined within GC hollow spheres. Among the investigated ratios,  $NiCo_2(S_{0.78}Se_{0.22})_5$  exhibited enhanced specific capacity of  $560.7\text{ C g}^{-1}$  at  $1\text{ A g}^{-1}$  and  $440.1\text{ C g}^{-1}$  at  $20\text{ A g}^{-1}$ , alongside pure sulfide and selenide. The constructed ASC utilizing the specified cathode and  $Bi_2O_{2.33}/rGO$  anode achieved an energy density of  $47.2\text{ Wh kg}^{-1}$  at  $801\text{ W kg}^{-1}$  and a capacity of  $212\text{ C g}^{-1}$  at  $1\text{ A g}^{-1}$ .

Recently, Lu et al. [181] presented an eco-friendly, safe, and straightforward approach to synthesize a bimetallic sulfoselenide–selenite heterojunction,  $(Ni,Co)(Se,S)_2/(Ni,Co)SeO_3$ , via a one-pot hydrothermal process with  $NiCo\text{-LDH}$  as a template. The coarse texture of the nanosheet array increases the number of active sites, while the multi-interface enhances the electronic structure for electrochemical processes. The optimized  $(Ni,Co)(Se,S)_2/(Ni,Co)SeO_3$  serves as a battery-type cathode for supercapacitors, demonstrating a high specific capacitance of  $7.61\text{ F cm}^{-2}$  at a current of  $2\text{ mA cm}^{-2}$ . The completed HSC device exhibits a high energy density of  $0.59\text{ mW h cm}^{-2}$  at a power density of  $1.44\text{ mW cm}^{-2}$  and demonstrates a capacitance retention rate of 84.38% after 5000 charge/discharge cycles.

In the following, Table 1 indicative performance metrics of representative MOF-based materials for supercapacitors are tabulated.

**Table 1.** Electrochemical performance indicators for MOF-based supercapacitor materials and devices.

Material(s)/Devices	Specific Capacitance or Capacity * [F/g] or [C/g] *	Energy Density [Wh/kg]	Power Density [W/kg]	Cycling Stability [% @ Cycles]	Ref.
Cu-MOF (sonochemically)	594.2	34.4	13,765	97.95 @ -	[39]
Ni-MOF derived $NiO/Ni/r\text{-GO}/r\text{-GO}$	172.2 *	39.6	41,360	80 @ 10,000	[72]
$NiCo\text{-PTA@PNTs}$	1109	41.2	375	79.1 @ 10,000	[182]
$NiO@Ni\text{-BTC/NF-12}$	1853 *	29.1	7000	94 @ 3000	[82]
Ni/Mn-PTA	2848	142.8	800	93.25 @ 5000	[183]
ZIF-8/ $Fe_2O_3//AC$	1160	28.5	2398	97 @ 1500	[87]
$Fe_3O_4@ZIF-67//AC$	1334.0	27.9	5488	87 @ 3000	[88]
ZIF-8/ZIF-67: 50/50	201	69	840	72 @ 5000	[184]
$MnO_2@NTO$	1054.7	36.2	11,879.9	85.3 @ 5000	[102]
Mn-PTA/NF	10.25	66	441	81.2 @ 10,000	[185]
$CoFe_2O_4@NiMn_2O_4/NF//AC$	312.8	90.3	12,900	88.4 @ 10,000	[120]
rGO/Ppy/Zn-MOF	175.0	19.7	1792	82 @ 7000	[137]
$NiCoP/C$ nanohybrids//AC	775.7	47.6	798.9	78.1 @ 10,000	[147]
$(Ni_{0.93}Mn_{0.07})_2P-18/CC$	851.1 *	59.8	750	84.87 @ 5000	[151]
$NiCo_2(S_{0.78}Se_{0.22})_5/GC//Bi_2O_{2.33}/rGO$	476.2	47.2		93.7 @ 100	[161]
Ni-MOF-24/ $Cu_3(HITP)_2/CFP$	1424	57	1500	94.3 @ 7000	[186]
Ni-CTP-COOH/GO	1258.7	79.7	1275	110 @ 5000	[187]

**Table 1.** *Cont.*

Material(s)/Devices	Specific Capacitance or Capacity * [F/g] or [C/g] *	Energy Density [Wh/kg]	Power Density [W/kg]	Cycling Stability [% @ Cycles]	Ref.
Cu-Co-MOF/rGO	935.8	45.2	2495.5	-	[188]
Cu-MOF/CNT Composite	348.56	27.7	1640	90.15 @ 10,000	[189]
Cu-MOF/CNT	166.4	23.6	501.5	79.2 @ 10,000	[190]
Cu-MOF/CNT // AC	1875 *	47	920	98.3 @ 15,000	[191]
NiMOF@MX 2 // AC (ASC)	1160.5	48.2	15,000	94 @ 10,000	[192]
Li-Cu-MOF // AC	171.1	36.1	5100	82.1 @ 1000	[193]

\* indicates specific capacity values.

### 3. Limitations and Outlook

Traditional MOFs possess fundamental drawbacks, particularly their limited conductivity and structural integrity, which constrain their application in electrochemical applications. However, specific challenges related to MOFs must be tackled to enable their broader commercialization. The inadequate electrochemical conductivity significantly restricts their potential applications, prompting the design and proposal of various nanocomposites with diverse structures across different dimensionalities.

The functionalization of MOF derivatives is still somewhat restricted; however, there exists significant potential to improve their electrochemical properties. This can be achieved by encapsulating functional groups and various species within their frameworks, aiming to develop high-performance energy storage devices through the identification of appropriate MOF derivatives for both anodes and cathodes in electrochemical devices.

Another possibility to improve MOF-based hybrid materials for electrochemical applications is the use of MXenes as hybrid components. MXenes have gained significant research interest in energy-storage applications arising from their exceptional metallic conductivity, superior hydrophilicity, unique layered structure, and abundant surface functional groups [194]. Nonetheless, MXenes have comparatively inferior thermodynamic and environmental stability in relation to MOFs [195]. As MXenes exhibit superior conductivity and satisfactory catalytic properties for electrochemical applications [196], consequent engineering the characteristics of the MOFs with MXenes can improve the electrical conductivity of the MOFs and at the same time increase the stability of the MXenes [197]. MXene/MOF-based composites have emerged also as excellent hydrophilic materials, facilitating immersion in aqueous electrolytes and quick charge transfer. As an example, the catalytic efficacy of CoBDC/MXene was assessed in alkaline, acidic, and neutral electrolytes, demonstrating low overpotentials of 29, 41, and 76 mV, respectively. To enhance comprehension of the operational mechanisms of these composites in energy storage and conversion, it is essential to refine and complete theoretical calculations and *in situ* characterizations. Nonetheless, numerous published studies exhibit a deficiency in comprehensive characteristic assessments and theoretical simulations of MXene/MOF composites and their derivatives [198]. MOFs are also an interesting alternative for the development of water-based electrolytes. The stability of MOFs in moisture as well as water is acknowledged as a critical characteristic concerning their prospective applications as the majority of MOFs exhibit a certain degree of water-lability. Aqueous energy devices necessitate metal–organic frameworks that exhibit exceptional stability in the presence of moisture and water. However, most MOFs exhibit low structural tolerance in aqueous systems. While MOFs and their derivatives have the potential to fulfill almost all essential criteria for use in aqueous energy devices, there are still challenges that must be addressed to achieve

greater success. While several MOFs have been developed exhibiting remarkable chemical and thermal stability, a need for further enhancement to withstand more extreme acidic or basic environments is required. The incorporation of guest molecules of appropriate dimensions could serve as a viable approach to improve the structural resilience of MOFs while preventing pore obstruction [199]. Another potential approach to address the degradation of MOFs in the presence of water is through surface hydrophobic modification [200].

MOF derivatives have surfaced as potential materials to tackle these limitations and discover applications across diverse electrochemical domains. These materials act as efficient templates, allowing for meticulous control over morphology, chemical modification, heteroatom doping, increased surface area, and structural alterations. There is huge progress potential for future applications that needs more attention by the research community.

In the future, the emphasis of exploration in MOFs might transition from traditional domains like storage or separation to more pressing and vital issues, such as the generation of clean energy. Notable progress has been made in improving the performance of MOF-based components to align with industrial and commercial standards. However, as mentioned above, further progress will require that MOFs surpass the standards set by conventional materials.

Transferring MOFs production technology from laboratory environments to commercial applications necessitates the capability to produce them at the appropriate quality, scale, and cost. Consequently, the principles of sustainable development and the circular economy are crucial, including the minimization of energy consumption, raw materials, reagent toxicity, and waste, as well as the design of materials for reuse and recyclability [201,202]. Transitioning from a batch to a continuous production process is significantly advantageous, as it facilitates expedited manufacturing (attributable to improved heat and mass transfer), enhanced reproducibility, diminished solvent and energy usage, increased space-time yield (STY) and reactor scalability, as well as decreased downtime and labor expenses (due to fewer steps between batches) [203]. The main issue in the scalability of MOFs production remains the price of the precursors. While some of them are not expensive (e.g., terephthalic acid or many metal precursors), more complex organic molecules can substantially increase the price of the final product.

In summary, the materials derived from MOFs demonstrate considerable promise and numerous advantages for application in energy production and storage systems. Considering the various existing challenges that are complex to tackle in the short term, a strong belief that a bright future awaits these innovative materials based on MOFs in real-world applications is maintained.

#### 4. Summary

This review concludes with the latest developments in MOFs-based materials for high-performance supercapacitor applications. It highlights how different synthesis strategies influence the morphologies and sizes of these materials, showcasing the extensive potential of MOFs to enhance electrochemical devices for energy storage. The connections between the electrochemical performances and the morphologies of the electrode active materials are highlighted. Additionally, the main challenges and viewpoints regarding materials based on MOFs and their derivatives for practical and sustainable electrochemical energy storage applications are briefly addressed.

MOFs exhibit a remarkable versatility, allowing for rational modifications tailored to meet various emerging needs. In this context, MOFs can play a significant role in advancing the hydrogen economy through their applications in electrocatalysis for hydrogen production and oxygen reduction, PEM fuel cells, and energy storage (rechargeable batteries

and supercapacitors). Their high surface areas (up to  $5.0 \times 10^3 \text{ m}^2 \text{ g}^{-1}$ ), highly uniform pores, adjustable pore geometries, adaptable structures, and diverse chemistry make MOFs compelling options for supercapacitor technologies. Furthermore, the use of multifunctional bridging ligands and post-synthetic modifications has enabled the careful design and functionalization of MOFs, facilitating the rational tuning of their properties. The wide range of possible combinations of metal centers and organic linkers allowing to design pores and increase active surface indicates a promising future for the application of MOFs in supercapacitors. The ability to manipulate pore structures alongside surface engineering could pave the way for a systematic investigation into how structural parameters and chemical compositions influence the performance of MOF-based electrochemical devices, potentially yielding important fundamental insights.

A significant body of work on MOFs and their derivatives has demonstrated and validated the consistency of their structures and chemical properties for current electrochemical applications at the laboratory scale. Nevertheless, additional advancements are essential, as numerous challenges in the realm of MOF-based electrochemical devices are currently being encountered and must be addressed promptly.

**Author Contributions:** Conceptualization, C.A. and G.S.; Validation, C.A., N.A. (Nikolaos Argirisis), N.A. (Niyaz Alizadeh) and G.S.; Investigation, C.A. and M.-E.K.; Data curation, C.A.; Writing—original draft preparation, C.A. and N.A. (Nikolaos Argirisis); Writing—review and editing, C.A., N.A. (Nikolaos Argirisis), N.A. (Niyaz Alizadeh), and M.-E.K.; Supervision, C.A. and G.S.; Project administration, G.S. All authors have read and agreed to the published version of the manuscript.

**Funding:** This research received no external funding.

**Data Availability Statement:** No new data has been produced for this work.

**Conflicts of Interest:** Authors Niyaz Alizadeh and Nikolaos Argirisis were affiliated with the company MAT4NRG. The remaining authors declare that the research was conducted in the absence of any commercial or financial relationships that could be construed as a potential conflict of interest.

## References

1. DNV As, Norway, Energy Transition Outlook 2024—A Global and Regional Forecast to 2050. Available online: [www.dnv.com](http://www.dnv.com) (accessed on 22 April 2025).
2. Wang, Y.; Wang, H.; Qu, G. Molybdenum-Based Electrode Materials Applied in High-Performance Supercapacitors. *Batteries* **2023**, *9*, 479. [[CrossRef](#)]
3. Qi, P.; Wang, H.; Lu, Y.; Chen, M.; Liu, G.; Li, W.; Huang, C.; Tang, Y. Ammonia-induced N-doped NiCoO<sub>2</sub> nanosheet array on Ni foam as a cathode of supercapacitor with excellent rate performance. *J. Alloys Compd.* **2022**, *895*, 162535. [[CrossRef](#)]
4. El-Shamy, O.A.A.; Siddiqui, M.R.; Mele, G.; Mohsen, Q.; Alhajeri, M.M.; Deyab, M.A. Synthesis, characterization and application of CNTs@Co-MOF and FCNTs@Co-MOF as superior supercapacitor: Experimental and theoretical studies. *J. Mol. Struct.* **2025**, *1321*, 140161. [[CrossRef](#)]
5. Kulkarni, O.; Bhosale, R.; Narale, D.; Pise, S.; Shaikh, T.; Kolekar, S. Dual redox center-based copper-cobalt metal–organic framework as pseudocapacitive electrode material for supercapacitor. *Inorg. Chem. Commun.* **2025**, *172*, 113711. [[CrossRef](#)]
6. Bojarajan, A.K.; Gunasekaran, S.S.; Kalluri, S.; Al Omari, S.A.B.; Bakenov, Z.; Sangaraju, S. Tuning capacitance of bimetallic ZnCo<sub>2</sub>O<sub>4</sub> using anionic, cationic and non-ionic surfactants by hydrothermal synthesis for high-performance asymmetric supercapacitor. *Inorg. Chem. Commun.* **2024**, *169*, 113035. [[CrossRef](#)]
7. Minakshi, M.; Samayamanthry, A.; Whale, J.; Aughterson, R.; Shinde, P.A.; Ariga, K.; Shrestha, L.K. Phosphorous—Containing Activated Carbon Derived from Natural Honeydew Peel Powers Aqueous Supercapacitors. *Chem. Asian J.* **2024**, *19*, e202400622. [[CrossRef](#)] [[PubMed](#)]
8. Minakshi, M.; Mujeeb, A.; Whale, J.; Evans, R.; Aughterson, R.; Shinde, P.A.; Ariga, K.; Shrestha Kumar, L. Synthesis of Porous Carbon Honeycomb Structures Derived from Hemp for Hybrid Supercapacitors with Improved Electrochemistry. *ChemPlusChem* **2024**, *89*, e202400408. [[CrossRef](#)]
9. Minakshi, M.; Wickramaarachchi, K. Electrochemical aspects of supercapacitors in perspective: From electrochemical configurations to electrode materials processing. *Prog. Solid State Chem.* **2023**, *69*, 100390. [[CrossRef](#)]

10. Alam, S.; Urooj, A.; Rehman, S.; Iqbal, M.Z.; Hegazy, H.H. Investigation of metal organic frameworks and their derivatives as electrode materials for hybrid energy storage devices. *Mater. Chem. Phys.* **2023**, *304*, 127877. [[CrossRef](#)]
11. Fleischmann, S.; Mitchell, J.B.; Wang, R.; Zhan, C.; Jiang, D.; Presser, V.; Augustyn, V. Pseudocapacitance: From fundamental understanding to high power energy storage materials. *Chem. Rev.* **2020**, *120*, 6738–6782. [[CrossRef](#)]
12. Brousse, T.; Belangér, D.; Long, J.W. To Be or Not To Be Pseudocapacitive? *J. Electrochem. Soc.* **2015**, *162*, A5185–A5189. [[CrossRef](#)]
13. Costentin, C.; Porter, T.R.; Savéant, J.-M. How do pseudocapacitors store energy? Theoretical analysis and experimental illustration. *ACS Appl. Mater. Interfaces* **2017**, *9*, 8649–8658. [[CrossRef](#)] [[PubMed](#)]
14. Kitagawa, S.; Kitaura, R.; Noro, S. Functional Porous Coordination Polymers. *Angew. Chem. Int. Ed.* **2004**, *43*, 2334–2375. [[CrossRef](#)] [[PubMed](#)]
15. Yaghi, O.M.; O’Keeffe, M.; Ockwig, N.W.; Chae, H.K.; Eddaoudi, M.; Kim, J. Reticular synthesis and the design of new materials. *Nature* **2003**, *423*, 705–714. [[CrossRef](#)]
16. Li, J.X.; Bao, T.; Zhang, C.; Song, H.; Zou, Y.Y.; Yuan, I.; Xi, Y.; Yu, C.Z.; Liu, C. A general strategy for direct growth of yolk-shell MOF-on-MOF hybrids. *Chem. Eng. J.* **2023**, *472*, 144926. [[CrossRef](#)]
17. Arbulu, R.C.; Jiang, Y.B.; Peterson, E.J.; Qin, Y. Metal-organic framework (MOF) nanorods, nanotubes, and nanowires. *Angew. Chem. Int. Ed.* **2018**, *57*, 5813–5817. [[CrossRef](#)]
18. Mohammadi, T.; Hosseini, M.G.; Rezvani Jalal, N.; Alavipour, E.; Pastor, E. Binder-free supercapacitors based on nanosheets of Bi-ligand Co metal-organic frameworks: Density functional theory validation. *J. Power Sources* **2025**, *632*, 236385. [[CrossRef](#)]
19. Furukawa, H.; Cordova, K.E.; O’Keeffe, M.; Yaghi, O.M. The Chemistry and Applications of Metal-Organic Frameworks. *Science* **2013**, *341*, 974. [[CrossRef](#)]
20. Lei, L.; Cheng, Y.; Chen, C.; Kosari, M.; Jiang, Z.; He, C. Taming structure and modulating carbon dioxide ( $\text{CO}_2$ ) adsorption isosteric heat of nickel-based metal organic framework (MOF-74(Ni)) for remarkable  $\text{CO}_2$  capture. *J. Colloid Interface Sci.* **2022**, *612*, 132–145. [[CrossRef](#)]
21. Zhang, W.; Bojdys, M.J.; Pinna, N. A universal synthesis strategy for tunable metal-organic framework nanohybrids. *Angew. Chem. Int. Ed.* **2023**, *62*, e202301021. [[CrossRef](#)]
22. Della Roca, J.; Liu, D.; Lin, W. Nanoscale Metal–Organic Frameworks for Biomedical Imaging and Drug Delivery. *Acc. Chem. Res.* **2011**, *44*, 957–968. [[CrossRef](#)] [[PubMed](#)]
23. Ren, Y.; Chia, G.H.; Gao, Z. Metal–organic frameworks in fuel cell technologies. *Nano Today* **2013**, *8*, 577–597. [[CrossRef](#)]
24. Zhang, H.; Lu, X.; Yang, L.; Hu, Y.; Yuan, M.; Wang, C.; Liu, Q.; Yue, F.; Zhou, D.; Xia, Q. Efficient air epoxidation of cycloalkenes over bimetal-organic framework ZnCoMOF materials. *Mol. Catal.* **2021**, *499*, 111300. [[CrossRef](#)]
25. Liang, Y.N.; Yao, W.G.; Duan, J.X.; Chu, M.; Sun, S.Z.; Li, X. Nickel cobalt bimetallic metal-organic frameworks with a layer-and-channel structure for high performance supercapacitors. *J. Energy Storage* **2021**, *33*, 102149. [[CrossRef](#)]
26. Lim, G.J.H.; Liu, X.M.; Guan, C.; Wang, J. Co/Zn bimetallic oxides derived from metal organic frameworks for high performance electrochemical energy storage. *Electrochim. Acta* **2018**, *291*, 177–187. [[CrossRef](#)]
27. Zhao, H.; Xu, W.; Li, M.; Meng, Z.; Ullah, I.; Nawaz, M.Z.; Wang, J.; Wang, C.; Chu, P.K. (Fe, Co) oxide nanowires on gold nanoparticles modified MOF-derived carbon nanoflakes for high-efficiency sodium-ion batteries and supercapacitors across electrolytes. *J. Power Sources* **2025**, *626*, 235793. [[CrossRef](#)]
28. Otun, K.O.; Diop, N.F.; Fasakin, O.; Adam, R.A.M.; Rutavi, G.; Manyala, N. Engineering the structures of ZnCo-MOFs via a ligand effect for enhanced supercapacitor performance. *RSC Adv.* **2025**, *15*, 4120–4136. [[CrossRef](#)]
29. Li, H.I.; Eddaoudi, M.; Keeffe, M.O.; Yaghi, O.M. Design and synthesis of an exceptionally stable and highly porous metal-organic framework. *Nature* **1999**, *402*, 276–279. [[CrossRef](#)]
30. Hao, X.; Song, W.; Wang, Y.; Qin, J.; Jiang, J. Recent Advancements in Electrochemical Sensors Based on MOFs and Their Derivatives. *Small* **2025**, *21*, 2408624. [[CrossRef](#)]
31. Xie, C.; Li, H.; Niu, B.; Guo, H.; Lin, X. Comparison of ultrasonic vs mechanochemistry methods for fabrication of mixed-ligand Zn-based MOFs for electrochemical determination of luteolin. *J. Alloys Compd.* **2024**, *989*, 174363. [[CrossRef](#)]
32. Kumar, R.S.; Kumar, S.S.; Kulandainathan, M.A. Efficient electrosynthesis of highly active Cu<sub>3</sub>(BTC)<sub>2</sub>-MOF and its catalytic application to chemical reduction. *Microporous Mesoporous Mater.* **2013**, *168*, 57–64. [[CrossRef](#)]
33. Kaur, G.; Kandwal Komal, P.; Sud, D. Sonochemically synthesized Zn (II) and Cd (II) based metal-organic frameworks as fluoroprobes for sensing of 2,6-dichlorophenol. *J. Solid State Chem.* **2023**, *319*, 123833. [[CrossRef](#)]
34. Glowniak, S.; Szczesniak, B.; Choma, J.; Jaroniec, M. Recent developments in sonochemical synthesis of nanoporous materials. *Molecules* **2023**, *28*, 2639. [[CrossRef](#)]
35. Mendes, R.F.; Rocha, J.; Almeida Paz, F.A. Chapter 8—Microwave Synthesis of Metal-Organic Frameworks. In *Metal-Organic Frameworks for Biomedical Applications*; Mozafari, M.B.T., Ed.; Woodhead Publishing: Cambridge, UK, 2020; pp. 159–176. [[CrossRef](#)]
36. Kumari, P.; Kareem, A.; Jharia, P.; Kumar, S.S.; Panda, T. Phase purity regulated by mechano-chemical synthesis of metal-organic frameworks for the electrocatalytic oxygen evolution reaction. *Inorg. Chem.* **2023**, *62*, 3457–3463. [[CrossRef](#)]

37. Wang, W.P.; Chai, M.; Zulkifli, M.Y.B.; Xu, K.J.; Chen, Y.L.; Wang, L.Z.; Chen, V.; Hou, J.W. Metal-organic framework composites from a mechanochemical process. *Mol. Syst. Des. Eng.* **2023**, *8*, 560–579. [[CrossRef](#)]
38. Vaitsis, C.; Kanellou, E.; Pandis, P.K.; Papamichael, I.; Sourkouni, G.; Zorbas, A.A.; Argirasis, C. Sonochemical synthesis of zinc adipate Metal-Organic Framework (MOF) for the electrochemical reduction of CO<sub>2</sub>: MOF and circular economy potential. *Sustain. Chem. Pharm.* **2022**, *29*, 100786. [[CrossRef](#)]
39. Shakeel, N.; Khan, J.; Al-Kahtani, A.A. Morphology-driven electrochemical attributes of Cu-MOF: A high-performance anodic material for battery supercapacitor hybrids. *RSC Adv.* **2024**, *14*, 33941–33951. [[CrossRef](#)]
40. Vaitsis, C.; Sourkouni, G.; Argirasis, C. Metal Organic Frameworks (MOFs) and ultrasound: A review. *Ultrason. Sonochemistry* **2019**, *52C*, 106–119. [[CrossRef](#)]
41. Muzaffar, N.; Afzal, A.M.; Hegazy, H.H.; Iqbal, M.W. Recent advances in two-dimensional metal-organic frameworks as an exotic candidate for the evaluation of redox-active sites in energy storage devices. *J. Energy Storage* **2023**, *64*, 107142. [[CrossRef](#)]
42. Zhang, G.; Jin, L.; Zhang, R.; Bai, Y.; Zhu, R.; Pang, P. Recent advances in the development of electronically and ionically conductive metal-organic frameworks. *Coord. Chem. Rev.* **2021**, *439*, 213915. [[CrossRef](#)]
43. Lee, S.J.; Telfer, S.G. Multicomponent metal-organic frameworks. *Angew. Chem. Int. Ed.* **2023**, *135*, e202306341. [[CrossRef](#)]
44. Lin, Z.X.; Richardson, J.J.; Zhou, J.J.; Caruso, F. Direct synthesis of amorphous coordination polymers and metal-organic frameworks. *Nat. Rev. Chem.* **2023**, *7*, 273–286. [[CrossRef](#)] [[PubMed](#)]
45. Wang, H.N.; Meng, X.; Dong, L.Z.; Chen, Y.; Li, S.L.; Lan, Y.Q. Coordination polymer-based conductive materials: Ionic conductivity vs. electronic conductivity. *J. Mater. Chem. A* **2019**, *7*, 24059–24091. [[CrossRef](#)]
46. Kumar, P.; Vellingiri, K.; Kim, K.-H.; Brown, R.J.C.; Manos, M.J. Modern progress in metal-organic frameworks and their composites for diverse applications. *Microporous Mesoporous Mater.* **2017**, *253*, 251–265. [[CrossRef](#)]
47. Bernales, V.; Ortuño, M.A.; Truhlar, D.G.; Cramer, C.J.; Gagliardi, L. Computational Design of Functionalized Metal–Organic Framework Nodes for Catalysis. *ACS Cent. Sci.* **2018**, *4*, 5–19. [[CrossRef](#)]
48. Coudert, F.X.; Fuchs, A.H. Computational characterization and prediction of metal–organic framework properties. *Coord. Chem. Rev.* **2016**, *307*, 211–236. [[CrossRef](#)]
49. McCarver, G.A.; Rajeshkumar, T.; Vogiatzis, K.D. Computational catalysis for metal-organic frameworks: An overview. *Coord. Chem. Rev.* **2021**, *436*, 213777. [[CrossRef](#)]
50. Hai, G.; Gao, H.; Huang, X.; Tan, L.; Xue, X.; Feng, S.; Wang, G. An efficient factor for fast screening of high-performance two-dimensional metal-organic frameworks towards catalyzing the oxygen evolution reaction. *Chem. Sci.* **2022**, *13*, 4397–4405. [[CrossRef](#)]
51. Chatterjee, P.; Sengul, M.Y.; Kumar, A.; MacKerell, A.D., Jr. Harnessing deep learning for optimization of Lennard-Jones parameters for the polarizable classical Drude oscillator force field. *J. Chem. Theory Comput.* **2022**, *18*, 2388–2407. [[CrossRef](#)]
52. Hai, G.; Wang, H. Theoretical studies of metal-organic frameworks: Calculation methods and applications in catalysis, gas separation, and energy storage. *Coord. Chem. Rev.* **2022**, *469*, 214670. [[CrossRef](#)]
53. Demir, H.; Daglar, H.; Gulbalkan, H.C.; Aksu, G.O.; Keskin, S. Recent advances in computational modeling of MOFs: From molecular simulations to machine learning. *Coord. Chem. Rev.* **2023**, *484*, 215112. [[CrossRef](#)]
54. Zhao, J.; Burke, A.F. Electrochemical capacitors: Materials, technologies and performance. *Energy Storage Mater.* **2021**, *36*, 31–55. [[CrossRef](#)]
55. Song, J.L.; Chai, L.; Kumar, A.; Zhao, M.; Sun, Y.Z.; Liu, X.G.; Pan, J.Q. Precise tuning of hollow and pore size of bimetallic MOFs derivate to construct high-performance nanoscale materials for supercapacitors and sodium-ion batteries. *Small* **2023**, *20*, 2306272. [[CrossRef](#)]
56. Kitchamsetti, N. A review on recent advances in Prussian blue, its analogues, and their derived materials as electrodes for high performance supercapacitors. *J. Energy Storage* **2023**, *73*, 108958. [[CrossRef](#)]
57. Xu, B.; Zhang, H.; Mei, H.; Sun, D. Recent progress in metal-organic framework-based supercapacitor electrode materials. *Coord. Chem. Rev.* **2020**, *420*, 213438. [[CrossRef](#)]
58. Yin, Z.; Wan, S.; Yang, J.; Kurmoo, M.; Zeng, M.-H. Recent advances in post-synthetic modification of metaleorganic frameworks: New types and tandem reactions. *Coord. Chem. Rev.* **2019**, *378*, 500–512. [[CrossRef](#)]
59. Li, C.; Sun, X.; Yao, Y.; Hong, G. Recent advances of electrically conductive metal-organic frameworks in electrochemical applications. *Mater. Today Nano* **2021**, *13*, 100105. [[CrossRef](#)]
60. Sundriyal, S.; Kaur, H.; Bhardwaj, S.K.; Mishra, S.; Kim, K.-H.; Deep, A. Metal-organic frameworks and their composites as efficient electrodes for supercapacitor applications. *Coord. Chem. Rev.* **2018**, *369*, 15–38. [[CrossRef](#)]
61. Chen, D.; Wei, L.; Li, J.; Wu, Q. Nanoporous materials derived from metal-organic framework for super-capacitor application. *J. Energy Storage* **2020**, *30*, 101525. [[CrossRef](#)]
62. Liu, Y.; Xu, X.; Shao, Z.; Jiang, S.P. Metal-organic frameworks derived porous carbon, metal oxides and metal sulfides-based compounds for supercapacitors application. *Energy Storage Mater.* **2020**, *26*, 1–22. [[CrossRef](#)]

63. Wang, Y.; Li, B.; Zhang, B.; Tian, S.; Yang, X.; Ye, H.; Xia, Z.; Zheng, G. Application of MOFs-derived mixed metal oxides in energy storage. *J. Electroanal. Chem.* **2020**, *878*, 114576. [[CrossRef](#)]
64. Li, S.; Luo, J.; Wang, J.; Zhu, Y.; Feng, J.; Fu, N.; Wang, H.; Guo, Y.; Tian, D.; Zheng, Y.; et al. Hybrid supercapacitors using metal-organic framework derived nickel-sulfur compounds. *J. Colloid Interface Sci.* **2024**, *669*, 265–274. [[CrossRef](#)]
65. Hao, Y.; Guo, H.; Yang, F.; Zhang, J.; Wu, N.; Wang, M.; Li, C.; Yang, W. Hydrothermal synthesis of MWCNT/Ni-Mn-S composite derived from bimetallic MOF for high-performance electrochemical energy storage. *J. Alloy. Compd.* **2022**, *911*, 164726. [[CrossRef](#)]
66. Qu, Y.; Sun, L.; Xie, F.; Hu, J.; Tan, H.; Zhang, Y. Metal-organic framework derived r-Ni<sub>3</sub>S<sub>2</sub> nanoparticles with enriched sulfur vacancies for supercapacitor application. *Appl. Surf. Sci.* **2023**, *623*, 157037. [[CrossRef](#)]
67. Lee, P.Y.; Lin, L.Y.; Yougbaré, S. Sulfurization of nickel-cobalt fluoride decorating ammonia ions as efficient active material of supercapacitor. *J. Solid State Chem.* **2022**, *313*, 123345. [[CrossRef](#)]
68. Naseer, M.; Siyal, S.H.; Najam, T.; Afzal, S.; Iqbal, R.; Ismail, M.A.; Rauf, A.; Shah, S.S.A.; Nazir, M.A. Engineering of metal oxide integrated metal organic frameworks (MO@ MOF) composites for energy and environment sector. *Mater. Sci. Eng. B* **2025**, *313*, 117909. [[CrossRef](#)]
69. Gao, Y.; Wu, J.; Zhang, W.; Tan, Y.; Zhao, J.; Tang, B. The electrochemical performance of SnO<sub>2</sub> quantum dots@zeolitic imidazolate frameworks-8 (ZIF-8) composite material for supercapacitors. *Mater. Lett.* **2014**, *128*, 208–211. [[CrossRef](#)]
70. Cui, H.; Liu, Y.; Ren, W.; Wang, M.; Zhao, Y. Large scale synthesis of highly crystallized SnO<sub>2</sub> quantum dots at room temperature and their high electrochemical performance. *Nanotechnology* **2013**, *24*, 345602. [[CrossRef](#)]
71. Yu, G.; Xie, X.; Pan, L.; Bao, Z.; Cui, Y. Hybrid nanostructured materials for high-performance electrochemical capacitors. *Nano Energy* **2013**, *2*, 213–234. [[CrossRef](#)]
72. Gowdhaman, A.; Kumar, S.A.; Elumalai, D.; Balaji, C.; Sabarinathan, M.; Ramesh, R.; Navaneethan, M. Ni-MOF derived NiO/Ni/r-GO nanocomposite as a novel electrode material for high-performance asymmetric supercapacitor. *J. Energy Storage* **2023**, *60*, 106769. [[CrossRef](#)]
73. Das, A.K.; Bera, R.; Maitra, A.; Karan, S.K.; Paria, S.; Halder, L.; Si, S.K.; Bera, A.; Khatua, B.B. Fabrication of an advanced asymmetric supercapacitor based on a microcubical PB@MnO<sub>2</sub> hybrid and PANI/GNP composite with excellent electrochemical behaviour. *J. Mater. Chem. A* **2017**, *5*, 22242–22254. [[CrossRef](#)]
74. Zhang, Y.Z.; Cheng, T.; Wang, Y.; Lai, W.Y.; Pang, H.; Huang, W. A simple approach to boost capacitance: Flexible supercapacitors based on manganese Oxides@MOFs via chemically induced in situ self-transformation. *Adv. Mater.* **2016**, *28*, 5242–5248. [[CrossRef](#)] [[PubMed](#)]
75. Zhang, L.; Zhang, Y.; Huang, S.; Yuan, Y.; Li, H.; Jin, Z.; Wu, J.; Liao, Q.; Hu, L.; Lu, J.; et al. Co<sub>3</sub>O<sub>4</sub>/Ni-based MOFs on carbon cloth for flexible alkaline battery-supercapacitor hybrid devices and near-infrared photocatalytic hydrogen evolution. *Electrochim. Acta* **2018**, *281*, 189–197. [[CrossRef](#)]
76. Zhang, F.; Zhang, J.; Song, J.; You, Y.; Jin, X.; Ma, J. Anchoring Ni-MOF nanosheet on carbon cloth by zeolite imidazole framework derived ribbonlike Co<sub>3</sub>O<sub>4</sub> as integrated composite cathodes for advanced hybrid supercapacitors. *Ceram. Int.* **2021**, *47*, 14001–14008. [[CrossRef](#)]
77. Zheng, J.H.; Zhang, R.M.; Yu, P.F.; Wang, X.G. Binary transition metal oxides (BTMO) (Co-Zn, Co-Cu) synthesis and high supercapacitor performance. *J. Alloys Compd.* **2019**, *772*, 359–365. [[CrossRef](#)]
78. Vaitsis, C.; Mechili, M.; Argiris, N.; Kanellou, E.; Pandis, P.K.; Sourkouni, G.; Zorbas, A.; Argiris, C. Ultrasound-Assisted preparation methods of nanoparticles for energy-related applications. In *Nanotechnology and the Environment*; Sen, M., Ed.; IntechOpen: London, UK, 2020; pp. 77–103. [[CrossRef](#)]
79. Shen, L.; Che, Q.; Li, H.; Zhang, X. Mesoporous NiCO<sub>2</sub>O<sub>4</sub> nanowire arrays grown on carbon textiles as binder-free flexible electrodes for energy storage. *Adv. Funct. Mater.* **2014**, *24*, 2630–2637. [[CrossRef](#)]
80. Wu, P.; Cheng, S.; Yao, M.; Yang, L.; Zhu, Y.; Liu, P.; Xing, O.; Zhou, J.; Wang, M.; Luo, H.; et al. A low-cost, self-standing NiCO<sub>2</sub>O<sub>4</sub>@CNT/CNT multilayer electrode for flexible asymmetric solid-state supercapacitors. *Adv. Funct. Mater.* **2017**, *27*, 1702160. [[CrossRef](#)]
81. Zhang, F.; Ma, J.; Yao, H. Ultrathin Ni-MOF nanosheet coated NiCO<sub>2</sub>O<sub>4</sub> nanowire arrays as a high-performance binder-free electrode for flexible hybrid supercapacitors. *Ceram. Int.* **2019**, *45*, 24279–24287. [[CrossRef](#)]
82. Xiong, S.; Jiang, S.; Wang, J.; Lin, H.; Lin, M.; Weng, S.; Liu, S.; Jiao, Y.; Xu, Y.; Chen, J. A high-performance hybrid supercapacitor with NiO derived NiO@Ni-MOF composite electrodes. *Electrochim. Acta* **2020**, *340*, 135956. [[CrossRef](#)]
83. Wang, J.; Zhong, Q.; Xiong, Y.; Cheng, D.; Zeng, Y.; Bu, Y. Fabrication of 3D Co-doped Ni-based MOF hierarchical micro-flowers as a high-performance electrode material for supercapacitors. *Appl. Surf. Sci.* **2019**, *483*, 1158–1165. [[CrossRef](#)]
84. Wang, Q.; Wang, Q.; Xu, B.; Gao, F.; Gao, F.; Zhao, C. Flower-shaped multiwalled carbon nanotubes@nickel-trimesic acid MOF composite as a high-performance cathode material for energy storage. *Electrochim. Acta* **2018**, *281*, 69–77. [[CrossRef](#)]

85. Li, N.; Li, Y.; Li, Q.; Zhao, Y.; Liu, C.S.; Pang, H. NiO nanoparticles decorated hexagonal Nickel-based metal-organic framework: Self-template synthesis and its application in electrochemical energy storage. *J. Colloid Interface Sci.* **2021**, *581 Pt B*, 709–718. [[CrossRef](#)]
86. Chen, J.; Xu, J.; Zhou, S.; Zhao, N.; Wong, C.-P. Template-grown graphene/porous Fe<sub>2</sub>O<sub>3</sub> nanocomposite: A high-performance anode material for pseudocapacitors. *Nano Energy* **2015**, *15*, 719–728. [[CrossRef](#)]
87. Chameh, B.; Moradi, M.; Hessari, F.A. Decoration of metal organic frameworks with FeO<sub>3</sub> for enhancing electrochemical performance of ZIF-(67 and 8) in energy storage application. *Synth. Met.* **2020**, *269*, 116540. [[CrossRef](#)]
88. Chameh, B.; Moradi, M.; Hajati, S.; Hessari, F.A. Design and construction of ZIF(8 and 67) supported Fe<sub>3</sub>O<sub>4</sub> composite as advanced materials of high performance supercapacitor. *Phys. E Low-Dimens. Syst. Nanostruct.* **2021**, *126*, 114442. [[CrossRef](#)]
89. Shabani Shayeh, J.; Salari, H. Dendritic fibrous nano metal organic framework: A magnetic core-shell structure as high performance material for electrochemical capacitors. *J. Energy Storage* **2020**, *32*, 101734. [[CrossRef](#)]
90. Albiter, E.; Merlano, A.S.; Rojas, E.; Barrera-Andrade, J.M.; Salazar, Á.; Valenzuela, M.A. Synthesis, characterization, and photocatalytic performance of ZnO-graphene nanocomposites: A review. *J. Compos. Sci.* **2020**, *5*, 4. [[CrossRef](#)]
91. Lee, K.M.; Lai, C.W.; Ngai, K.S.; Juan, J.C. Recent developments of zinc oxide based photocatalyst in water treatment technology: A review. *Water Res.* **2016**, *88*, 428–448. [[CrossRef](#)]
92. Sulciute, A.; Nishimura, K.; Gilshtein, E.; Cesano, F.; Viscardi, G.; Nasibulin, A.G.; Ohno, Y.; Rackauskas, S. ZnO nanostructures application in electrochemistry: Influence of morphology. *J. Phys. Chem. C* **2021**, *125*, 1472–1482. [[CrossRef](#)]
93. Luo, W.; Zhang, Q.; Zhang, J.; Moioli, E.; Zhao, K.; Züttel, A. Electrochemical reconstruction of ZnO for selective reduction of CO<sub>2</sub> to CO. *Appl. Catal. B Environ.* **2020**, *273*, 119060. [[CrossRef](#)]
94. Saranya, M.; Ramachandran, R.; Wang, F. Graphene-zinc oxide (G-ZnO) nanocomposite for electrochemical supercapacitor applications. *J. Sci. Adv. Mater. Dev.* **2016**, *1*, 454–460. [[CrossRef](#)]
95. Liu, Y.N.; Jin, L.N.; Wang, H.T.; Kang, X.H.; Bian, S.W. Fabrication of three-dimensional composite textile electrodes by metal-organic framework, zinc oxide, graphene and polyaniline for all-solid-state supercapacitors. *J. Colloid Interface Sci.* **2018**, *530*, 29–36. [[CrossRef](#)] [[PubMed](#)]
96. Zhu, C.; He, Y.; Liu, Y.; Kazantseva, N.; Saha, P.; Cheng, Q. ZnO@MOF@PANI core-shell nanoarrays on carbon cloth for high-performance supercapacitor electrodes. *J. Energy Chem.* **2019**, *35*, 124–131. [[CrossRef](#)]
97. Zuhri, F.U.; Diantoro, M.; Suryanti, L.; Suprayogi, T.; Nasikhudin, S.; Meevasana, W. ZnO-FC-NiCo MOF for prospective supercapacitor materials. *Mater. Today Proc.* **2021**, *44*, 3385–3389. [[CrossRef](#)]
98. Reghunath, S.; Pinheiro, D.; Kr, S.D. A review of hierarchical nanostructures of TiO<sub>2</sub>: Advances and applications. *Appl. Surf. Sci. Adv.* **2021**, *3*, 100063. [[CrossRef](#)]
99. Ramasubbu, V.; Omar, F.S.; Ramesh, K.; Ramesh, S.; Shajan, X.S. Three-dimensional hierarchical nano-structured porous TiO<sub>2</sub> aerogel/Cobalt based metal-organic framework (MOF) composite as an electrode material for supercapattery. *J. Energy Storage* **2020**, *32*, 101750. [[CrossRef](#)]
100. Feng, J.; Feng, J.; Zhang, C. Thermal conductivity of low density carbon aerogels. *J. Porous Mater.* **2011**, *19*, 551–556. [[CrossRef](#)]
101. Keshavarz, L.; Ghaani, M.R.; MacElroy, J.M.D.; English, N.J. A comprehensive review on the application of aerogels in CO<sub>2</sub>-adsorption: Materials and characterization. *Chem. Eng. J.* **2021**, *412*, 128604. [[CrossRef](#)]
102. Kitchamsetti, N.; Samtham, M.; Singh, D.; Choudhary, E.; Rondiya, S.R.; Ma, Y.R.; Cross, R.W.; Dzade, N.Y.; Devan, R.S. Hierarchical 2D MnO<sub>2</sub>@1D mesoporous NiTiO<sub>3</sub> core-shell hybrid structures for high-performance supercapattery electrodes: Theoretical and experimental investigations. *J. Electroanal. Chem.* **2023**, *936*, 117359. [[CrossRef](#)]
103. Khan, M.W.; Khan, A.S.; Rohma; Pai, S.H.S.; Mohapatra, G.; Kumar, A.; Ali, R.B.; Sial, Q.A.; Seo, H. Electrodeposition of redox active nickel-manganese metal organic framework and manganese sulfide composite for supercapacitors. *Electrochim. Acta* **2025**, *513*, 145554. [[CrossRef](#)]
104. Feng, G.; Zhao, T.; Zhou, L.; Wang, X.; Ding, H.; Jiang, F.; Li, H.; Liu, Y.; Yu, Q.; Cao, H.; et al. Nanocubic transition metal sulfides (FeMn)S<sub>2</sub>@NC synthesized by MOFs facile for supercapacitors. *Vacuum* **2025**, *231*, 113819. [[CrossRef](#)]
105. Kim, M.K.; Kim, W.J.; Kim, M.L.; Ahn, G.H.; Hong, J.P.; Ryu, G.H.; Hong, J. Hierarchically structured transition metal (Cu, Ni) sulfide core-shell electrode for high-performance supercapacitor. *J. Alloys Compd.* **2025**, *1014*, 178717. [[CrossRef](#)]
106. Lu, P.; Jiang, X.; Guo, W.; Wang, L.; Zhang, T.; Boyjoo, Y.; Si, W.; Hou, F.; Liu, J.; Dou, S.X.; et al. A Ni-Co sulfide nanosheet/carbon nanotube hybrid film for high-energy and high-power flexible supercapacitors. *Carbon* **2021**, *178*, 355–362. [[CrossRef](#)]
107. Liu, Y.; Huang, D.; Cheng, M.; Liu, Z.; Lai, C.; Zhang, C.; Zhou, C.; Xiong, W.; Qin, L.; Shao, B.; et al. Metal sulfide/MOF-based composites as visible-light-driven photocatalysts for enhanced hydrogen production from water splitting. *Coord. Chem. Rev.* **2020**, *409*, 213220. [[CrossRef](#)]
108. Song, X.Z.; Zhang, N.; Wang, X.F.; Tan, Z. Recent advances of metal-organic frameworks and their composites toward oxygen evolution electrocatalysis. *Mater. Today Energy* **2021**, *19*, 100597. [[CrossRef](#)]
109. Lee, C.S.; Lim, J.M.; Park, J.T.; Kim, J.H. Direct growth of highly organized, 2D ultra-thin nano-accordion Ni-MOF@NiS<sub>2</sub>@C core-shell for high performance energy storage device. *Chem. Eng. J.* **2021**, *406*, 126810. [[CrossRef](#)]

110. Zhang, J.; Li, Y.; Han, M.; Xia, Q.; Chen, Q.; Chen, M. Constructing ultra-thin Ni-MOF@NiS<sub>2</sub> nanosheets arrays derived from metal organic frameworks for advanced all-solid-state asymmetric supercapacitor. *Mater. Res. Bull.* **2021**, *137*, 111186. [[CrossRef](#)]
111. Yue, L.; Wang, X.; Sun, T.; Liu, H.; Li, Q.; Wu, N.; Guo, H.; Yang, W. Ni-MOF coating MoS<sub>2</sub> structures by hydrothermal intercalation as high-performance electrodes for asymmetric supercapacitors. *Chem. Eng. J.* **2019**, *375*, 121959. [[CrossRef](#)]
112. Wei, J.; Hu, F.; Shen, X.; Chen, B.; Chen, L.; Wang, Z.; Lv, C.; Ouyang, Q. Defective core–shell NiCO<sub>2</sub>S<sub>4</sub>/MnO<sub>2</sub> nanocomposites for high performance solid-state hybrid supercapacitors. *J. Colloid Interface Sci.* **2023**, *649*, 665–674. [[CrossRef](#)]
113. Ali, M.; Afzal, A.M.; Iqbal, M.W.; Mumtaz, S.; Imran, M.; Ashraf, F.; Rehman, A.U.; Muhammad, F. 2D-TMDs based electrode material for supercapacitor applications. *Int. J. Energy Res.* **2022**, *46*, 22336–22364. [[CrossRef](#)]
114. Wang, J.; Li, S.; Zhu, Y.; Zhai, S.; Liu, C.; Fu, N.; Hou, S.; Niu, Y.; Luo, J.; Mu, S.; et al. Metal-organic frameworks-derived NiSe@RGO composites for high-performance hybrid supercapacitors. *J. Electroanal. Chem.* **2022**, *919*, 116548. [[CrossRef](#)]
115. Zhang, N.; Meng, Q.; Wu, H.; Hu, X.; Zhang, M.; Zhou, A.; Li, Y.; Huang, Y.; Li, L.; Wu, F.; et al. Co-MOF as Stress-Buffered Architecture: An engineering for improving the performance of NiS/SnO<sub>2</sub> heterojunction in lithium storage. *Adv. Energy Mater.* **2023**, *13*, 2300413. [[CrossRef](#)]
116. Hu, M.-L.; Masoomi, M.Y.; Morsali, A. Template strategies with MOFs. *Coord. Chem. Rev.* **2019**, *387*, 415–435. [[CrossRef](#)]
117. Mei, J.; Liao, T.; Ayoko, G.A.; Bell, J.; Sun, Z. Cobalt oxide-based nanoarchitectures for electrochemical energy applications. *Prog. Mater. Sci.* **2019**, *103*, 596–677. [[CrossRef](#)]
118. Chen, T.-Y.; Lin, L.-Y.; Geng, D.-S.; Lee, P.-Y. Systematic synthesis of ZIF-67 derived Co<sub>3</sub>O<sub>4</sub> and N-doped carbon composite for supercapacitors via successive oxidation and carbonization. *Electrochim. Acta* **2021**, *376*, 137986. [[CrossRef](#)]
119. Xu, J.; Liu, S.; Liu, Y. Co<sub>3</sub>O<sub>4</sub>/ZnO nanoheterostructure derived from core-shell ZIF-8@ZIF-67 for supercapacitors. *RSC Adv.* **2016**, *6*, 52137–52142. [[CrossRef](#)]
120. Kitchamsetti, N.; Kim, D. High performance hybrid supercapacitor based on hierarchical MOF derived CoFe<sub>2</sub>O<sub>4</sub> and NiMn<sub>2</sub>O<sub>4</sub> composite for efficient energy storage. *J. Alloys Compd.* **2023**, *959*, 170483. [[CrossRef](#)]
121. Iqbal, M.Z.; Zakir, A.; Shoukat, W.; Badi, N.; Afzal, A.M.; Fouada, A.M.; Hegazy, H.H. Enhancing the electrochemical efficiency of metal-organic frameworks through integration of chromium nitride interfacial layer for efficient hybrid supercapacitors. *J. Energy Storage* **2025**, *105*, 114606. [[CrossRef](#)]
122. Wang, B.; Tan, W.; Fu, R.; Mao, H.; Kong, Y.; Qin, Y.; Tao, Y. Hierarchical mesoporous Co<sub>3</sub>O<sub>4</sub>/C@MoS<sub>2</sub> core-shell structured materials for electrochemical energy storage with high supercapacitive performance. *Synth. Met.* **2017**, *233*, 101–110. [[CrossRef](#)]
123. Hou, S.; Lian, Y.; Bai, Y.; Zhou, Q.; Ban, C.; Wang, Z.; Zhao, J.; Zhang, H. Hollow dodecahedral Co<sub>3</sub>S<sub>4</sub>@NiO derived from ZIF-67 for supercapacitor. *Electrochim. Acta* **2020**, *341*, 136053. [[CrossRef](#)]
124. Zhao, J.; Li, H.; Li, C.; Zhang, Q.; Sun, J.; Wang, X.; Guo, J.; Xie, L.; Xie, J.; He, B.; et al. MOF for template-directed growth of well-oriented nanowire hybrid arrays on carbon nanotube fibers for wearable electronics integrated with triboelectric nanogenerators. *Nano Energy* **2018**, *45*, 420–431. [[CrossRef](#)]
125. Prasad Ojha, G.; Muthurasu, A.; Prasad Tiwari, A.; Pant, B.; Chhetri, K.; Mukhiya, T.; Dahal, B.; Lee, M.; Park, M.; Kim, H.-Y. Vapor solid phase grown hierarchical Cu<sub>x</sub>O NWs integrated MOFs-derived CoS<sub>2</sub> electrode for high-performance asymmetric supercapacitors and the oxygen evolution reaction. *Chem. Eng. J.* **2020**, *399*, 125532. [[CrossRef](#)]
126. Govindan, R.; Hong, X.-J.; Sathishkumar, P.; Cai, Y.-P.; Gu, F.L. Construction of metal-organic framework-derived CeO<sub>2</sub>/C integrated MoS<sub>2</sub> hybrid for high-performance asymmetric supercapacitor. *Electrochim. Acta* **2020**, *353*, 136502. [[CrossRef](#)]
127. Gayathri, S.; Arunkumar, P.; Saha, D.; Han, J.H. Composition engineering of ZIF-derived cobalt phosphide/cobalt monoxide heterostructures for high-performance asymmetric supercapacitors. *J. Colloid Interface Sci.* **2021**, *588*, 557–570. [[CrossRef](#)]
128. Hu, X.; Zhang, S.; Sun, J.; Yu, L.; Qian, X.; Hu, R.; Wang, Y.; Zhao, H.; Zhu, J. 2D Fe-containing cobalt phosphide/cobalt oxide lateral heterostructure with enhanced activity for oxygen evolution reaction. *Nano Energy* **2019**, *56*, 109–117. [[CrossRef](#)]
129. Wang, J.; Gao, R.; Zheng, L.; Chen, Z.; Wu, Z.; Sun, L.; Hu, Z.; Liu, X. CoO/CoP heterostructured nanosheets with an O-P interpenetrated Interface as a bifunctional electrocatalyst for Na-O<sub>2</sub> battery. *ACS Catal.* **2018**, *8*, 8953–8960. [[CrossRef](#)]
130. Guo, J.W.; Zhao, H.B.; Yang, Z.W.; Wang, Y.W.; Liu, X.L.; Wang, L.F.; Zhao, Z.H.; Wang, A.Z.; Ding, L.H.; Liu, H.; et al. Hierarchical porous 3D Ni<sub>3</sub>N-CoN/NC heterojunction nanosheets with nitrogen vacancies for high-performance flexible supercapacitor. *Nano Energy* **2023**, *116*, 108763. [[CrossRef](#)]
131. Zhao, J.J.; Liu, N.; Sun, Y.Z.; Xu, Q.H.; Pan, J.Q. Nitrogen-modified spherical porous carbon derived from aluminum-based metal-organic frameworks as activation-free materials for supercapacitors. *J. Energy Storage* **2023**, *73*, 109070. [[CrossRef](#)]
132. Zhang, S.; Dai, P.; Liu, H.; Yan, L.; Song, H.; Liu, D.; Zhao, X. Metal-organic framework derived porous flakes of cobalt chalcogenides (CoX, X = O, S, Se and Te) rooted in carbon fibers as flexible electrode materials for pseudocapacitive energy storage. *Electrochim. Acta* **2021**, *369*, 137681. [[CrossRef](#)]
133. Zhang, A.; Zhang, Q.; Fu, H.C.; Zong, H.W.; Guo, H.W. Metal-organic frameworks and their derivatives based nanostructure with different dimensionalities for supercapacitors. *Small* **2023**, *19*, 2303911. [[CrossRef](#)]

134. Kumar, S.; Kumar, V.; Bulla, M.; Devi, R.; Dahiya, R.; Sisodiya, A.K.; Singh, R.B.; Mishra, A.K. Hydrothermally reduced graphene oxide based electrodes for high-performance symmetric supercapacitor. *Mater. Lett.* **2024**, *364*, 136364. [[CrossRef](#)]
135. Feng, W.; Liu, C.; Liu, Z.; Pang, H. In-situ growth of N-doped graphene-like carbon/MOF nanocomposites for high-performance supercapacitor. *Chin. Chem. Lett.* **2024**, *35*, 109552. [[CrossRef](#)]
136. Kausar, A.; Ahmad, I. Graphene-MOF hybrids in high-tech energy devices—Present and future advances. *Hybrid Adv.* **2024**, *5*, 100150. [[CrossRef](#)]
137. Saxena, N.; Bondarde, M.P.; Lokhande, K.D.; Bhakare, M.A.; Dhumal, P.S.; Some, S. One-pot synthesis of rGO/Ppy/Zn-MOF, ternary composite for High-Performance supercapacitor application. *Chem. Phys. Lett.* **2024**, *856*, 141605. [[CrossRef](#)]
138. Lian, P.C.; Liu, H.H.; Li, H.; Zhang, Y.; Mei, Y. A facile and mild route to synthesize ultralight and flexible 3D functionalized graphene. *J. Porous. Mater.* **2018**, *25*, 905–911. [[CrossRef](#)]
139. Tang, Z.; Lei, Y.; Deng, Y.; Chen, J.; Liu, K.; Zhang, C.; Wang, T.; Lei, Y. MOF-derived MoS<sub>2</sub>/nitrogen-doped graphene aerogel for supercapacitor electrodes. *Diam. Relat. Mater.* **2025**, *153*, 112098. [[CrossRef](#)]
140. Siddiqui, R.; Rani, M.; Shah, A.A.; Razaq, A.; Iqbal, R.; Neffati, R.; Arshad, M. Fabrication of tricarboxylate-neodymium metal organic frameworks and its nanocomposite with graphene oxide by hydrothermal synthesis for a symmetric supercapacitor electrode material. *Mater. Sci. Eng. B* **2023**, *295*, 116530. [[CrossRef](#)]
141. Ashraf, M.; Umar, E.; Sunny, M.A.; Iqbal, M.W.; Hassan, H.; Alrobei, H.; Ismayilova, N.A.; Alawaideh, Y.M.; Al-Buraihi, M.S.; Alomairy, S. Reduced graphene oxides embedded zeolitic imidazolate framework-8 and copper sulfide as electrodes for asymmetric supercapacitors and hydrogen evolution reactions. *J. Energy Storage* **2024**, *104*, 114479. [[CrossRef](#)]
142. Kumar, R.V.; Vickraman, P.; Raja, T.A.; Bharathi, M.S.R. Exploratory mass dispersoid rGO in-situ influence on nickel phosphate-trimesic acid metal-organic framework for higher energy density hybrid supercapacitors. *J. Energy Storage* **2024**, *102*, 114140. [[CrossRef](#)]
143. Hassan, H.; Shoib, M.; Khan, K.; Ghanem, M.A.; Osman, M. Graphene quantum dots decorated on chromium oxide and zirconium metal-organic framework composite (GQDs@Zr-MOF/Cr<sub>2</sub>O<sub>3</sub>) for asymmetric supercapacitors and hydrogen production. *Mater. Chem. Phys.* **2025**, *332*, 130225. [[CrossRef](#)]
144. Xiong, C.; Zhang, Y.; Zheng, C.; Yin, Y.; Xiong, Q.; Zhao, M.; Wang, B. Fabrication of metal-organic framework@cellulose nanofibers/reduced graphene oxide-Vitrimer composite electrode materials with shape memory for supercapacitors. *Electrochim. Acta* **2024**, *493*, 144373. [[CrossRef](#)]
145. Wang, H.; Wang, L.; Zhao, P.; Zhang, X.; Lu, X.; Qiu, Z.; Qi, B.; Yao, R.; Huang, Y.; Wang, L.; et al. Metal-organic framework-mediated construction of confined ultrafine nickel phosphide immobilized in reduced graphene oxide with excellent cycle stability for asymmetric supercapacitors. *J. Colloid Interface Sci.* **2023**, *649*, 616–625. [[CrossRef](#)]
146. Tang, X.R.; Li, N.; Pang, H. Metal-organic frameworks-derived metal phosphides for electrochemistry application. *Green Energy Environ.* **2022**, *7*, 636–661. [[CrossRef](#)]
147. Zhou, Q.; Gong, Y.; Tao, K. Calcination/phosphorization of dual Ni/Co-MOF into NiCoP/C nanohybrid with enhanced electrochemical property for high energy density asymmetric supercapacitor. *Electrochim. Acta* **2019**, *320*, 134582. [[CrossRef](#)]
148. Liu, S.; Xu, W.; Feng, K.; Shi, X.; Xu, Z.; Teng, R.; Fan, X.; Wang, C. Three-dimensional heterostructured nickel phosphide @ nickel cobalt phosphide nanocomposites with highly porous surface for high-performance supercapacitor. *Colloids Surf. A Physicochem. Eng. Asp.* **2024**, *686*, 133342. [[CrossRef](#)]
149. Yi, M.; Lu, B.; Zhang, X.; Tan, Y.; Zhu, Z.; Pan, Z.; Zhang, J. Ionic liquid-assisted synthesis of nickel cobalt phosphide embedded in N, P codoped-carbon with hollow and folded structures for efficient hydrogen evolution reaction and supercapacitor. *Appl. Catal. B Environ.* **2021**, *283*, 119635. [[CrossRef](#)]
150. Zhu, Y.; Lao, J.; Xu, F.; Sun, L.; Shao, Q.; Luo, Y.; Fang, S.; Chen, Y.; Yu, C.; Zou, Y. A structurally controllable flower-shaped phosphide derived from metal-organic frameworks for high-performance supercapacitors. *J. Electroanal. Chem.* **2024**, *966*, 118376. [[CrossRef](#)]
151. Liu, S.; Xu, W.; Feng, K.; Shi, X.; Wang, C. Bimetallic MOF derived NiMn phosphide for high-performance supercapacitor electrode material. *J. Energy Storage* **2024**, *96*, 112684. [[CrossRef](#)]
152. Zhou, H.; Nasser, R.; Zhang, L.; Li, Z.; Li, F.; Song, J.-M. Copper/Cobalt based metal phosphide composites as positive material for supercapacitors. *Chem. Eng. J.* **2024**, *496*, 154102. [[CrossRef](#)]
153. Lao, J.; Zhu, Y.; Xu, F.; Sun, L.; Fang, S.; Shao, Q.; Liao, L.; Guan, Y.; Zou, Y. A novel 1D MXene fibers-loaded metal-organic framework derived bimetallic sulfide for high-performance supercapacitors. *Fuel* **2024**, *362*, 130904. [[CrossRef](#)]
154. Ramesh, S.; Rabani, I.; Sivasamy, A.; Kakani, V.; Haldorai, Y.; Seo, Y.-S.; Kim, J.-H.; Kim, H.S. Fabrication of nickel-copper sulfide nanoparticles decorated on metal-organic framework composite for supercapacitor application by hydrothermal process. *J. Alloys Compd.* **2024**, *977*, 173375. [[CrossRef](#)]
155. Guo, H.; Zhang, H.; Wu, N.; Pan, Z.; Li, C.L.; Chen, Y.; Cao, Y.J.; Yang, W. Trimesic acid-modified 2D NiCo-MOF for high-capacity supercapacitors. *J. Alloys Compd.* **2023**, *934*, 167779. [[CrossRef](#)]

156. Liu, Y.; Li, Y.; Kang, H.; Jin, T.; Jiao, L. Design, synthesis, and energy-related applications of metal sulfides. *Mater. Horiz.* **2016**, *3*, 402–421. [CrossRef]
157. Ouyang, Y.; Zhang, B.; Wang, C.; Xia, X.; Lei, W.; Hao, Q. Bimetallic metal-organic framework derived porous NiCo<sub>2</sub>S<sub>4</sub> nanosheets arrays as binder-free electrode for hybrid supercapacitor. *Appl. Surf. Sci.* **2021**, *542*, 148621. [CrossRef]
158. Wang, D.; Tian, L.; Huang, J.; Li, D.; Liu, J.; Xu, Y.; Ke, H.; Wei, Q. “One for two” strategy to prepare MOF- derived NiCo<sub>2</sub>S<sub>4</sub> nanorods grown on carbon cloth for high-performance asymmetric supercapacitors and efficient oxygen evolution reaction. *Electrochim. Acta* **2020**, *334*, 135636. [CrossRef]
159. Cai, P.; Liu, T.; Zhang, L.; Cheng, B.; Yu, J. ZIF-67 derived nickel cobalt sulfide hollow cages for high-performance supercapacitors. *Appl. Surf. Sci.* **2020**, *504*, 144501. [CrossRef]
160. Li, G.-C.; Liu, M.; Wu, M.-K.; Liu, P.-F.; Zhou, Z.; Zhu, S.-R.; Liu, R.; Han, L. MOF-derived self-sacrificing route to hollow NiS<sub>2</sub>/ZnS nanospheres for high performance supercapacitors. *RSC Adv.* **2016**, *6*, 103517–103522. [CrossRef]
161. Cai, F.; Sun, R.; Kang, Y.; Chen, H.; Chen, M.; Li, Q. One-step strategy to a three-dimensional NiS-reduced graphene oxide hybrid nanostructure for high performance supercapacitors. *RSC Adv.* **2015**, *5*, 23073–23079. [CrossRef]
162. Ruan, Y.; Jiang, J.; Wan, H.; Ji, X.; Miao, L.; Peng, L.; Zhang, B.; Lv, L.; Liu, J. Rapid self-assembly of porous square rod-like nickel persulfide via a facile solution method for high-performance supercapacitors. *J. Power Sources* **2016**, *301*, 122–130. [CrossRef]
163. Shrivastav, V.; Sundriyal, S.; Goel, P.; Shrivastav, V.; Tiwari, U.K.; Deep, A. ZIF-67 derived Co<sub>3</sub>S<sub>4</sub> hollow microspheres and WS<sub>2</sub> nanorods as a hybrid electrode material for flexible 2V solid-state supercapacitor. *Electrochim. Acta* **2020**, *345*, 136194. [CrossRef]
164. Zhao, W.; Yan, G.; Zheng, Y.; Liu, B.; Jia, D.; Liu, T.; Cui, L.; Zheng, R.; Wei, D.; Liu, J. Bimetal-organic framework derived Cu(NiCo)S<sub>4</sub>/Ni<sub>3</sub>S<sub>4</sub> electrode material with hierarchical hollow heterostructure for high performance energy storage. *J. Colloid Interface Sci.* **2020**, *565*, 295–304. [CrossRef] [PubMed]
165. Li, M.D.; Jiang, X.Y.; Liu, J.J.; Liu, Q.; Lv, N.J.; Qi, N.; Chen, Z.Q. A flower-like Co/Ni bimetallic metal-organic framework based electrode material with superior performance in supercapacitors. *J. Alloys Compd.* **2023**, *930*, 167354. [CrossRef]
166. Xiong, D.; Gu, M.; Chen, C.; Lu, C.; Yi, F.-Y.; Ma, X. Rational design of bimetallic metal-organic framework composites and their derived sulfides with superior electrochemical performance to remarkably boost oxygen evolution and supercapacitors. *Chem. Eng. J.* **2021**, *404*, 127111. [CrossRef]
167. Nataraj, N.; Dash, P.; Sakthivel, R.; Lin, Y.-C.; Fang, H.-W.; Chung, R.-J. Simultaneous electrochemical and colorimetric detection of tri-heavy metal ions in environmental water samples employing 3D-MOF/nickel selenide as a synergistic catalyst. *Chem. Eng. J.* **2024**, *485*, 149965. [CrossRef]
168. Al-Shaibah, F.N.; Ibrahim, M.A.A.; Abu Hatab, A.S.; Abotaleb, A.; Sinopoli, A.; Zekri, A.; Ahmad, Y.H.; Al-Qaradawi, S.Y. Rational synthesis of MOF-Derived Cobalt-Based binary selenides nanocrystals for electrochemical oxygen evolution reaction. *Appl. Surf. Sci.* **2025**, *688*, 162479. [CrossRef]
169. Sheikhi, S.; Jalali, F. Copper selenide—Porous carbon derived from metal-organic frameworks as an efficient electrocatalyst for methanol oxidation. *Int. J. Hydrogen Energy* **2024**, *55*, 864–874. [CrossRef]
170. Zhai, Z.; Yan, W.; Dong, L.; Wang, J.; Chen, C.; Lian, J.; Wang, X.; Xia, D.; Zhang, J. Multi-dimensional materials with layered structures for supercapacitors: Advanced synthesis, supercapacitor performance and functional mechanism. *Nano Energy* **2020**, *78*, 105193. [CrossRef]
171. Zhang, Y.; Pan, A.; Wang, Y.; Cao, X.; Zhou, Z.; Zhu, T.; Liang, S.; Cao, G. Self-templated synthesis of N-doped CoSe<sub>2</sub>/C double-shelled dodecahedra for high-performance supercapacitors. *Energy Storage Mater.* **2017**, *8*, 28–34. [CrossRef]
172. Mei, H.; Zhang, L.; Zhang, K.; Gao, J.; Zhang, H.; Huang, Z.; Xu, B.; Sun, D. Conversion of MOF into carbon-coated NiSe<sub>2</sub> yolk-shell microspheres as advanced battery-type electrodes. *Electrochim. Acta* **2020**, *357*, 136866. [CrossRef]
173. Wang, Q.; Ran, X.; Shao, W.; Miao, M.; Zhang, D. High performance flexible supercapacitor based on metal-organic-framework derived CoSe<sub>2</sub> nanosheets on carbon nanotube film. *J. Power Sources* **2021**, *490*, 229517. [CrossRef]
174. Sun, P.; Zhang, J.; Huang, J.; Wang, L.; Wang, P.; Cai, C.; Lu, M.; Yao, Z.; Yang, Y. Bimetallic MOF-derived (CuCo)Se nanoparticles embedded in nitrogen-doped carbon framework with boosted electrochemical performance for hybrid supercapacitor. *Mater. Res. Bull.* **2021**, *137*, 111196. [CrossRef]
175. Li, Z.; Tian, M.; Chen, Y.; Liu, Y.; Cai, Y.; Wei, W. MOFs derived (Ni<sub>0.75</sub>Co<sub>0.25</sub>)Se<sub>2</sub> nanoparticles embedded in N-doped nanocarbon for hybrid supercapacitors. *Ceram. Int.* **2021**, *47*, 12623–12630. [CrossRef]
176. Acharya, J.; Ojha, G.P.; Pant, B.; Park, M. Construction of self-supported bimetallic MOF-mediated hollow and porous tri-metallic selenide nanosheet arrays as battery-type electrodes for high-performance asymmetric supercapacitors. *J. Mater. Chem. A* **2021**, *9*, 23977–23993. [CrossRef]
177. Dong, W.; Li, X.; Ye, F.; Xu, X.; Zhang, X.; Yang, F.; Shen, D.; Hong, X.; Yang, S. Synergistically enhanced multimetallic selenide electrode materials derived from ZIF-67 templates for high-performance supercapacitors. *J. Energy Storage* **2025**, *114*, 115870. [CrossRef]

178. Charis Caroline, S.; Das, B.; Pramana, S.S.; Batabyal, S.K. Nickel sulfide-nickel sulfoselenide nanosheets as a potential electrode material for high performance supercapacitor with extended shelf life. *J. Energy Storage* **2023**, *68*, 107812. [[CrossRef](#)]
179. Zhao, Y.; Wang, S.; Ye, F.; Liu, W.; Lian, J.; Li, G.; Wang, H.; Hu, L.; Wu, L. Hierarchical mesoporous selenium@bimetallic selenide quadrilateral nanosheet arrays for advanced flexible asymmetric supercapacitors. *J. Mater. Chem. A* **2022**, *10*, 16212–16223. [[CrossRef](#)]
180. Yi, M.; Wu, A.; Chen, Q.; Cai, D.; Zhan, H. In situ confined conductive nickel cobalt sulfoselenide with tailored composition in graphitic carbon hollow structure for energy storage. *Chem. Eng. J.* **2018**, *351*, 678–687. [[CrossRef](#)]
181. Lu, X.; Chen, Q.; Wu, L.; Cui, S.; Li, G.; Zhao, W.; Han, L. A multi-interface bimetallic sulfoselenide–selenite heterojunction as a battery-type cathode for high-performance supercapacitors. *New J. Chem.* **2024**, *48*, 15227–15239. [[CrossRef](#)]
182. Huang, S.; Shi, X.-R.; Sun, C.; Duan, Z.; Ma, P.; Xu, S. The Application of Metal–Organic Frameworks and Their Derivatives for Supercapacitors. *Nanomaterials* **2020**, *10*, 2268. [[CrossRef](#)]
183. Lan, M.; Wang, X.; Zhao, R.; Dong, M.; Fang, L.; Wang, L. Metal-organic framework-derived porous MnNi<sub>2</sub>O<sub>4</sub> microflower as an advanced electrode material for high-performance supercapacitors. *J. Alloys Compd.* **2020**, *821*, 153546. [[CrossRef](#)]
184. Javed, M.S.; Aslam, M.K.; Asim, S.; Batool, S.; Idrees, M.; Hussain, S.; Shah, S.S.A.; Saleem, M.; Mai, W.; Hu, C. High-performance flexible hybrid-supercapacitor enabled by pairing binder-free ultrathin Ni–Co–O nanosheets and metal-organic framework derived N-doped carbon nanosheets. *Electrochim. Acta* **2020**, *349*, 136384. [[CrossRef](#)]
185. Liu, J.; Wang, Z.; Bi, R.; Mao, F.; Wang, K.; Wu, H.; Wang, X. A polythreaded MnII-MOF and its super-performances for dye adsorption and supercapacitors. *Inorg. Chem. Front.* **2020**, *7*, 718–730. [[CrossRef](#)]
186. Deng, T.; Shi, X.; Zhang, W.; Wang, Z.; Zheng, W. In-plane Assembly of Distinctive 2D MOFs with Optimum Supercapacitive Performance. *iScience* **2020**, *23*, 101220. [[CrossRef](#)] [[PubMed](#)]
187. Shi, X.; Yu, J.; Liu, Q.; Shao, L.; Zhang, Y.; Sun, Z.; Huang, H. Metal-Organic-Framework-Derived N-, P-, and O-Codoped Nickel/Carbon Composites Homogeneously Decorated on Reduced Graphene Oxide for Energy Storage. *ACS Appl. Nano Mater.* **2020**, *3*, 5625–5636. [[CrossRef](#)]
188. Maliha, Z.; Rani, M.; Neffati, R.; Mahmood, A.; Iqbal, M.Z.; Shah, A. Investigation of copper/cobalt MOFs nanocomposite as an electrode material in supercapacitors. *Int. J. Energy Res.* **2022**, *46*, 17404–17415. [[CrossRef](#)]
189. Singh, M.K.; Krishnan, S.; Singh, K.; Rai, D.K. CNT Interwoven Cu-MOF: A Synergistic Electrochemical Approach for Solid-State Supercapacitor and Hydrogen Evolution Reaction. *Energy Fuels* **2024**, *38*, 12098–12110. [[CrossRef](#)]
190. Anwer, A.H.; Ansari, M.Z.; Mashkoor, F.; Zhu, S.; Shoeb, M.; Jeong, C. Synergistic effect of carbon nanotube and tri-metallic MOF nanoarchitecture for electrochemical high-performance asymmetric supercapacitor applications and their charge storage mechanism. *J. Alloys Compd.* **2023**, *955*, 170038. [[CrossRef](#)]
191. Zaka, A.; Iqbal, M.W.; Afzal, A.M.; Hassan, H.; Alharthi, S.; Amin, M.A.; Saeedi, A.M.; Albargi, H.B.; Alhadrami, A.; Alqarni, N.D.; et al. Synergistic innovations in energy Storage: Cu-MOF infused with CNT for supercapattery devices and hydrogen evolution reaction. *Inorg. Chem. Commun.* **2024**, *159*, 111739. [[CrossRef](#)]
192. Ji, Y.; Li, W.; You, Y.; Xu, G. In situ synthesis of M (Fe, Cu, Co and Ni)-MOF@MXene composites for enhanced specific capacitance and cyclic stability in supercapacitor electrodes. *Chem. Eng. J.* **2024**, *496*, 154009. [[CrossRef](#)]
193. Iqbal, M.Z.; Aziz, U.; Aftab, S.; Wabaidur, S.M.; Siddique, S.; Iqbal, M.J. A Hydrothermally Prepared Lithium and Copper MOF Composite as Anode Material for Hybrid Supercapacitor Applications. *Angew. Chem.* **2023**, *8*, e202204554. [[CrossRef](#)]
194. Suganthi, S.; Ahmad, K.; Oh, T.H. Progress in MOFs and MOFs-Integrated MXenes as Electrode Modifiers for Energy Storage and Electrochemical Sensing Applications. *Molecules* **2024**, *29*, 5373. [[CrossRef](#)] [[PubMed](#)]
195. Do, H.H.; Cho, J.H.; Han, S.M.; Ahn, S.H.; Kim, S.Y. Metal–Organic-Framework- and MXene-Based Taste Sensors and Glucose Detection. *Sensors* **2021**, *21*, 7423. [[CrossRef](#)]
196. Su, H.; Jin, C.; Zhang, X.; Yu, Z.; Zeng, X. Recent progress in the synthesis and electrocatalytic application of MXene-based metal phosphide composites. *Carbon Neutralization* **2024**, *3*, 1009–1035. [[CrossRef](#)]
197. Basha, S.I.; Shah, S.S.; Helal, A.; Aziz, M.A.; Yoo, D.-Y. Unveiling the limitless potential: Exploring metal–organic frameworks (MOFs)/MXene based construction materials. *Case Stud. Constr. Mater.* **2024**, *21*, e03586. [[CrossRef](#)]
198. Yang, H.; Zhang, G.-X.; Zhou, H.-J.; Sun, Y.-Y.; Pang, H. Metal–Organic Frameworks Meet MXene: New Opportunities for Electrochemical Application. *Energy Mater. Adv.* **2023**, *4*, 0033. [[CrossRef](#)]
199. Tan, H.; Zhou, Y.; Qiao, S.-Z.; Fan, H.J. Metal organic framework (MOF) in aqueous energy devices. *Mater. Today* **2021**, *48*, 270–284. [[CrossRef](#)]
200. Ding, M.; Jiang, H.-L. Improving Water Stability of Metal–Organic Frameworks by a General Surface Hydrophobic Polymerization. *CCS Chem.* **2021**, *3*, 2740–2748. [[CrossRef](#)]
201. Woodliffe, J.L.; Molinar-Díaz, J.; Clowes, R.; Hussein, O.H.; Lester, E.; Ferrari, R.; Ahmed, I.; Laybourn, A. Continuous flow synthesis of MOF UTSA-16(Zn), mixed-metal and magnetic composites for CO<sub>2</sub> capture—Toward scalable manufacture. *J. Environ. Chem. Eng.* **2024**, *12*, 114167. [[CrossRef](#)]

202. Woodliffe, J.L.; Ferrari, R.S.; Ahmed, I.; Laybourn, A. Evaluating the purification and activation of metal-organic frameworks from a technical and circular economy perspective. *Coord. Chem. Rev.* **2021**, *428*, 213578. [[CrossRef](#)]
203. Laybourn, A.; Robertson, K.; Slater, A.G. Quid pro flow. *J. Am. Chem. Soc.* **2023**, *145*, 4355–4365. [[CrossRef](#)]

**Disclaimer/Publisher's Note:** The statements, opinions and data contained in all publications are solely those of the individual author(s) and contributor(s) and not of MDPI and/or the editor(s). MDPI and/or the editor(s) disclaim responsibility for any injury to people or property resulting from any ideas, methods, instructions or products referred to in the content.